Naval Research Laboratory

Washington, DC 20375-5000

NRL Memorandum Report 6767

Three Dimensional Variable Constraint Effects in Fracture Initiation

V. G. DEGIORGI

Mechanics of Materials Branch
Materials Science and Technology Division

March 25, 1991

REPORT DOCUMENTATION PAGE

Form Approved
OMB No. 0704-0188

1. AGENCY USE ONLY (Leave blank)	2. REPORT DATE	3. REPORT TYPE AND DATES COVERED
	1991 March 25	

4. TITLE AND SUBTITLE

Three Dimensional Variable Constraint Effects in Fracture Initiation

5. FUNDING NUMBERS

PE - 61153N
PR - RR022-01-48

6. AUTHOR(S)

V. G. DeGiorgi

7. PERFORMING ORGANIZATION NAME(S) AND ADDRESS(ES)

Naval Research Laboratory
Washington, DC 20375-5000

8. PERFORMING ORGANIZATION REPORT NUMBER

NRL Memorandum
Report 6767

9. SPONSORING/MONITORING AGENCY NAME(S) AND ADDRESS(ES)

10. SPONSORING/MONITORING AGENCY REPORT NUMBER

11. SUPPLEMENTARY NOTES

12a. DISTRIBUTION/AVAILABILITY STATEMENT

Approved for public release; distribution unlimited.

12b. DISTRIBUTION CODE

13. ABSTRACT *(Maximum 200 words)*

Many naturally occurring cracks are three dimensional and cannot be evaluated using numerical techniques derived using two dimensional simplifications. The high stress and strain levels experienced in modern high toughness alloys prior to fracture require means to accurately simulate the nonlinear material response in this regime. An accurate constitutive representation must be combined with a fracture criterion which is valid for the high strain regime to achieve accurate numerical simulations of fracture and near fracture behavior. In the current work, nonlinear numerical simulations are performed to determine the global and local responses of two surface cracked plates of HY-100 steel with varying crack depths. Failure is defined by a local fracture criterion using strain energy density. Differences in constraint along the crack perimeter are taken into account by recognizing the stress-strain history dependence of the critical strain energy density. Crack growth patterns determined from the numerical simulations accurately reflect experimental observations.

14. SUBJECT TERMS			15. NUMBER OF PAGES
Surface crack	Fracture		56
Part-through crack	Finite element		16. PRICE CODE
Strain energy density			

17. SECURITY CLASSIFICATION OF REPORT	18. SECURITY CLASSIFICATION OF THIS PAGE	19. SECURITY CLASSIFICATION OF ABSTRACT	20. LIMITATION OF ABSTRACT
UNCLASSIFIED	UNCLASSIFIED	UNCLASSIFIED	UL

CONTENTS

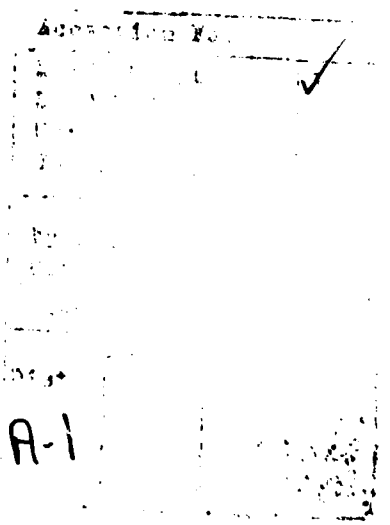

THREE DIMENSIONAL VARIABLE CONTRAINT EFFECTS IN FRACTURE INITIATION

Introduction

Many naturally occurring cracks do not extend the entire width of the specimen or component. The study of these partial or surface cracks is important for structural integrity evaluations. Numerous investigations into the surface crack problem have been conducted over the years. While straight cracks which span the entire thickness are amenable to 2D analytical and numerical evaluations, surface cracks in general require full 3D analytical and numerical evaluations. The high stress and strain levels which occur at the crack tip region require accurate constitutive representations for this regime of the material response spectrum. The need for detailed 3D nonlinear numerical representations results in expensive and time consuming numerical simulations. The level of detail necessary to establish the variation along the curved crack tip requires access to large computing facilities. Numerical and analytical difficulties which limited the study of surface cracks in linear elastic materials and materials which exhibit only a relatively small amount of inelastic strain prior to fracture have made the study of surface cracks in ductile materials all but intractable. Recent advances in numerical methods and computer capabilities have made the study of surface cracks in ductile materials more feasible.

The ability to accurately predict fracture initiation and subsequent failure relies on the ability to accurately predict the magnitude of the stress, strain and energy fields surrounding the crack tip. The variation in stress, strain and energy along the irregular crack front is important in determining fracture initiation sites, ductile tearing patterns and fatigue crack growth characteristics. The location of fracture inititaion along the crack perimeter is equally as important as global failure parameters such as load or crack mouth opening displacement (CMOD). Crack growth patterns are important because the shape of a surface crack effects its criticality. For instance, a surface crack which grows deep and narrow instead of deep and wide is more likely to lead to leak before break conditions in a piping system [1].

The absolute and relative dimensions of a surface flaw are also important. Larger surface flaws will tend to lead to fracture due to the presence of the crack whereas a smaller surface flaw may have a minimal effect and failure will result from gross global instabilities. "Larger" and "smaller" are used in a relative sense. Global geometry, loading conditions, material toughness as well as crack dimensions will determine, for a specific geometry and material, the extent of "larger" and "smaller."

Numerous analytical, experimental and computational studies have been completed on surface cracks over the past three decades. The current

Manuscript approved December 28, 1990.

summary is not meant to be an exhaustive literature review of the surface crack problem.

One of the major difficulties in the study of surface cracks is the infinite number of crack shapes possible. The shape of a surface crack is dependent on component geometry, local material inhomogeneties, material toughness and applied loading among other factors. There are some geometric simplifications which can be used.While not exact representations of the irregular boundary of many cracks, semi-elliptical crack fronts can be used to approximate the shape of natural cracks [2,3]. A semi-elliptical surface crack representation and angular definitions used in the current analysis are shown in Figure 1.

Even with limiting the surface crack shape to semi-elliptical a wide range of geometries still exist. In order to narrow the geometry selection process one of three general approaches may be taken. The first approach is to model a specific geometry, both crack and component. The advantage with this approach is that a specific applications problem has been solved. The disadvantage is that the information obtained is geometry, material and component specific. Examples of this approach are studies of surface cracks in cylinders [4], studies of surface cracks in cylindrical tee-sections such as found in piping systems [5] and studies of surface flaws in nozzle corners [6].

The second analysis approach is to examine typical flaws from numerous sources to determine if there are surface crack geometries which are statistically significant. Numerical simulations would then be performed on these statistically significant crack geometries. A disadvantage with this analysis approach is the nature of the available data. There are many data summaries of observed surface cracks but the collected data is for particular component geometries, materials and loading conditions. Much data is obtained only after failure or significant growth [7,8]. One analysis which used statistical methods was an effort to determine the critical features of crack geometry and the inadequacy of a semi-elliptical representation [9].

A second disadvantage with determining a statistically significant crack geometry is that significant crack geometry may not be the initial geometry but may be one which results after some ductile or fatigue crack growth. As part of the general study of surface crack behavior and criticality, fatigue crack growth patterns have been documented (Figure 2) [10,11]. It has been shown that surface cracks will tend to growth towards certain aspect ratios depending on initial geometry and loading conditions. However, these final aspect ratios occur at relatively deep crack depths (greater than 70%) and may not be reached prior to fracture.

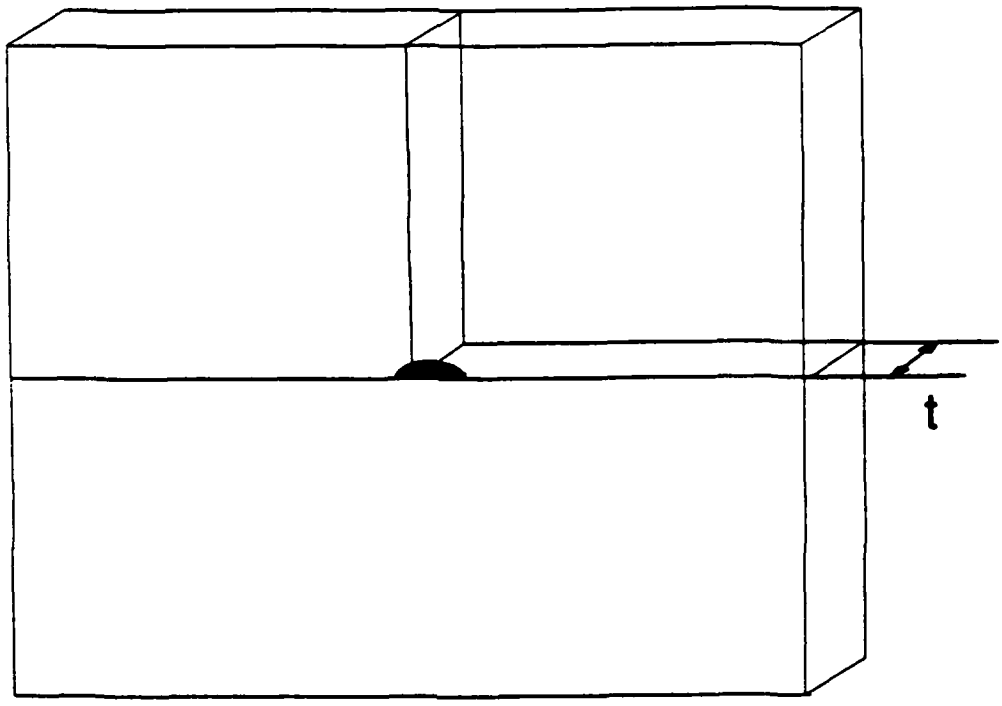

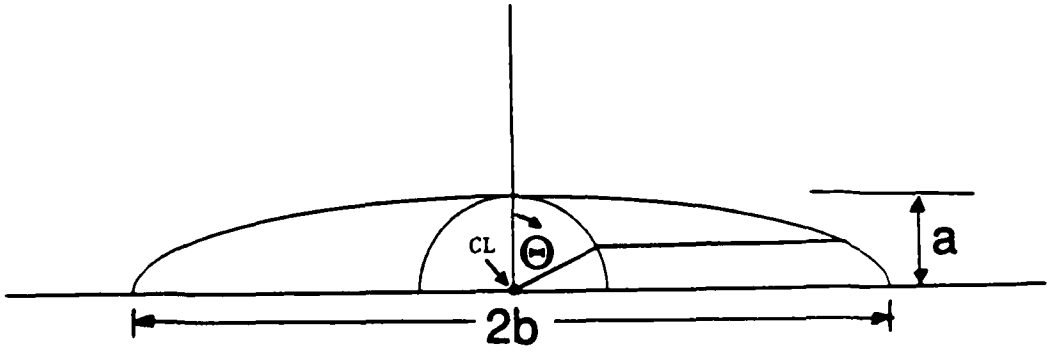

Fig. 1 — Typical Surface Crack Geometry — Semi-Elliptical Representation

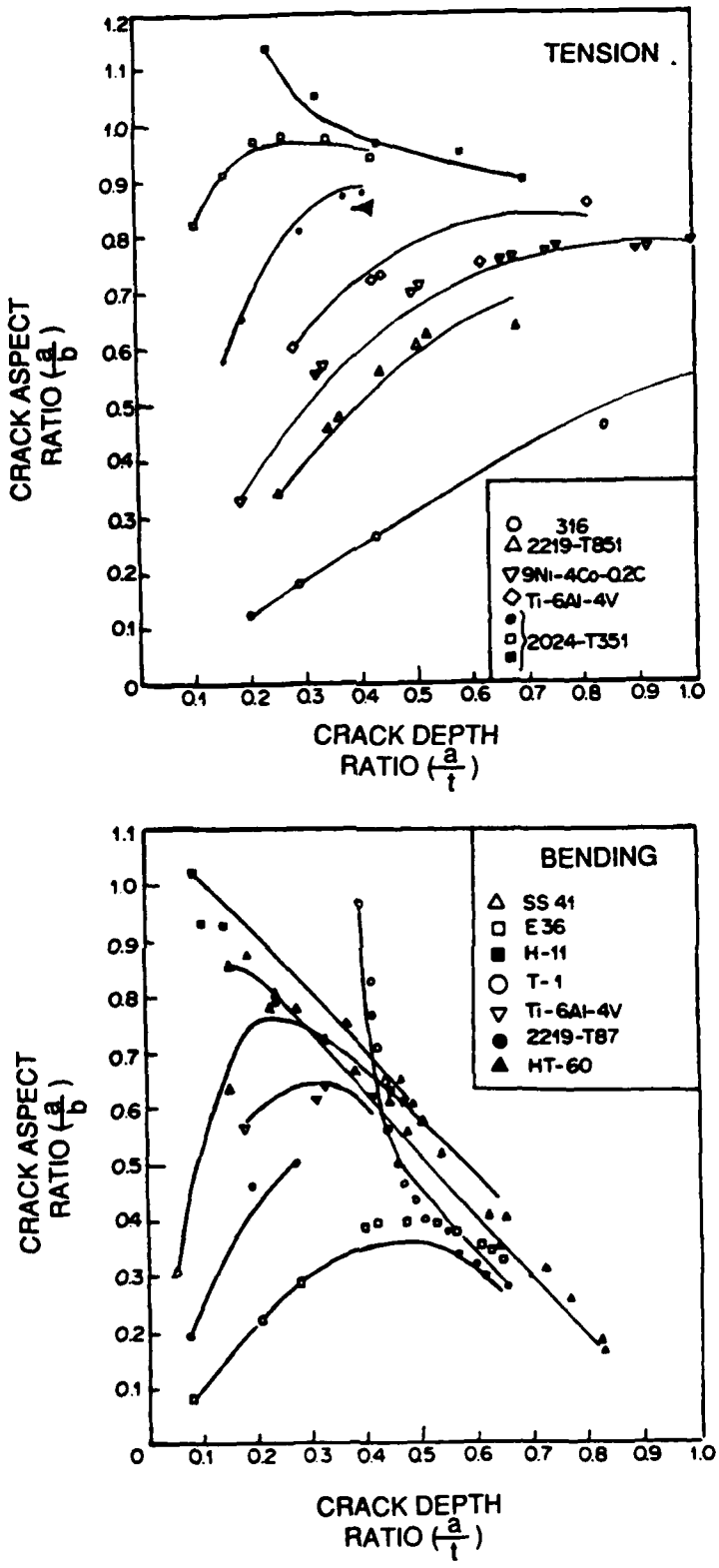

Fig. 2 — Fatigue Crack Growth Patterns per Shang-Xian [11]

In the first two analysis approaches there is considerable difficulty in isolating the effects on the stress, strain and energy fields which are solely attributable to the surface crack. Geometric and material effects are embedded into the application problem approach and in the data from which a statistically significant crack geometries must be determined.

The third analysis approach is the study of several surface crack geometries in geometrically simple components fabricated from a particular material of interest. The material chosen should be representative of a class of materials. The material response to loading should be well understood. The advantage in this approach is that an attempt is made to keep all factors, except for the surface crack geometry, identical. This will allow for the comparison of results for different surface crack geometries. In this manner the influence of a surface crack on the stress, strain and energy in a component may be examined. The disadvantage is that numerous analyses are required to determine the effects of a wide range of surface crack geometries. This is the approach taken by many researchers, including work on HRR field dominance by Parks and Wang [12] and J-integral studies by Dodds and Read [13].

This analysis approach is followed in the current work. Two crack geometries, one semi-circular and one semi-elliptical, are evaluated using numerical simulation techniques. The stress, strain and energy fields along the curved crack perimeter are examined for three crack depths. Moderate crack depths are studied. The surface crack is embedded in HY-100 structural steel and independently subjected to tension or bending loads. HY-100 structural steel is a high toughness, high ductility alloy used in current structural applications.

Background

Numerous linear elastic fracture mechanics (LEFM) analyses of surface cracks have been performed. Among the methods used for determination of the critically of a surface crack are empirical formulations for the stress intensity factor [14], weight functions based on reference stress intensity factors which allow for arbitrary loading conditions [15], analytical solutions which incorporate through crack solutions[16], boundary element evaluation of the cracked component [17] and finite element evaluations [18]. Linear elastic analyses methods are only appropriate for elastic material behavior or in cases where only a limited amount of plasticity occurs at the crack tip. They are not appropriate for the evaluation of ductile high strength

materials, such as HY-100 steel, which exhibit large amounts of deformation and strain prior to fracture initiation.

While not strictly valid in the study of fracture in ductile materials, surface flaw characteristics and growth behaviors based on LEFM analyses are invaluable when studying surface flaw behavior. Hodulak, Kordisch and Sommer postulated that surface crack growth was in reality a two part problem [19]: the determination of stress intensity for LEFM applications and the determination of crack growth resistance. The crack growth resistance, or material toughness, is considered by Hodulak, Kordisch and Sommer to be a variable quantity along the curved crack front. The variation in crack resistance is attributed to interactions between the stress state and material response and is affected by component geometry, degree of loading and the nature of loading. This model of surface crack growth consists of a surface crack in a plate with layers of different crack resistance. The crack resistance is greater in the surface layers to capture the free surface effects. Crack growth will increase once the crack has penetrated the regions of lower resistance. The crack will show a tendency to stabilizes its growth rate until it reaches the higher resistance layer associated with the rear surface. Until the surface crack encounters the rear surface layer of higher resistance growth in the thickness layer will dominate. Experimental verification of this crack growth model has been performed [19,20]. Surface cracks with a range of aspect ratios were tested under cases of simple tension. Surface cracks tested were contained in aluminum alloy plates and reactor steel cylinders. Results common to both geometries are:

for shallow and moderate depth cracks ($a/t < 0.5$) crack growth in the thickness direction dominates

for deeper cracks, growth in the width direction dominates

growth patterns for surface cracks were found to be similar for plates and cylinders

It is important to note that the extent of the variable resistant layers is not qualitatively defined. The crack growth models used where based on LEFM response.

In contrast to the approach adopted by Hodulak et al [20], other researchers have worked with the assumption that the critical value of the chosen fracture criteria is constant. Trantina et al [21] have performed a 3-D finite element analysis of a shallow semi-circular surface crack. The finite element model is subjected to several levels of monotonically applied remote strain varying from elastic to 1.35 times the strain associated with the yield

stress. J-integral values were determined at several positions along the crack perimeter. The stress intensity factor, K, profile was determined by converting the J-integral values to K values using assumptions of small-scale yielding. The K values were compared with Newman-Raju LEFM calculated K values [14]. Significant differences are observed between these two K profiles. The maximum Newman-Raju LEFM K value occurs at the free surface. The maximum K for the finite element analysis occurs approximately 75° from the crack centerline. The results of this analysis were used to model the change in crack shape with growth. For an initially semi-circular crack, crack growth would result in a retardation along the free surface and the final crack geometry would be indented along the free surface. This is consistent with experimental observations. It is important to note that, even though the finite element analysis incorporates significant amounts of plasticity, LEFM relationships of J-integral and K values are utilized.

VanStone et al [22] used the work of Trantina et al to establish a cyclic load crack growth model. The crack growth model developed is a variation of the Newman-Raju LEFM K profile along the crack perimeter which incorporates a reduction in K at the free surface. K was reduced proportional to the size of the plastic zone at the free surface. Empirical constants were determined for the model from surface crack and through crack specimens. The lives predicted by the model were within a factor of two of experimental values. Patterns of crack growth predicted were similar to those observed experimentally. It should be noted that the applied nominal stress was less than the yield strength of the material. Net section yielding was avoided. The analysis performed while not strictly LEFM is in the range of loading where LEFM results have been found to be useful.

In the majority of surface crack fracture initiation and growth studies performed, as typified by those summarized above, the surface crack failure parameter is assumed constant and the crack resistance is assume to vary along the crack perimeter. This variation is either represented by changes in the material toughness (the increased resistance layer of Hodulak et al) or modifications of the fracture parameter (the constraint loss model of VanStone et al). The failure criteria is typically determined for two points along the curved crack perimeter - the deepest point and at the free surface. The surface crack is assumed to grow in a semi-elliptical manner. The aspect ratio is allowed to change with crack growth however the overall general shape of the crack is maintained.

Extension of the surface crack problem into the regime of ductile material response increases the complexity of the problem. The J-integral,

one of the standard single parameter fracture criteria for 2D problems, has been modified for application to the surface flaw problem. 3D J and J-type parameters have been derived by Dodds et al [23], Dodds and Read [13] and Nishishkov and Atluri [24] among others. An empirical modification of J-integral for surface cracks has been presented by Dodds and Read [13]. In all derived 3D J and J-type parameters there is the underlying assumption that the crack tip stress field will be an HRR stress field near the crack tip as in the 2D J integral derivation. Parks and Wang [12] performed a very detailed 3D nonlinear finite element analysis for a variety of plate geometries containing deep surface cracks range from 50 to 60% through the thickness. Material response was modeling using deformation theory plasticity based on a Ramberg-Osgood constitutive relationship. It was determined that significant variations from HRR stress field dominance in the Mode I dominate stress component occurs for nominal applied stresses near the yield stress. J and J-type parameters require HRR stress field dominance. The implication of this work is that J and J-type parameters are not adequate to describe fracture along a surface crack in ductile materials.

The lack of HRR dominance for deeper cracks at near yield remote tension stress levels complicates the use of J and J-type criteria. Even though an HRR stress field may occur for shallower surface cracks it is not possible to use a criteria based on HRR stresses for the entire range of crack depths. The range of J or J-type parameter validity must be determined. The use of strain energy density as the continuum fracture criteria for surface cracks does not require any additional verification of the form of the state of stress, strain or energy in the vicinity of the crack tip at any crack depth considerations. The strain energy density is determined from the generalized stress and strain tensors. The six components of stress and strain are explicitly incorporated into the strain energy density. The critical strain energy density as determined from a series of cylindrical tensile tests is based on the individual stress and strain components present at failure. The determined value of strain energy density is not affected by mathematical form which represents the stress or strain field, therefore HRR dominance is not an issue.

Analysis Objectives

In the current analysis, two surface cracks of different aspect ratios embedded in HY-100 steel plates are examined in detail for various depths. The depths are representative of moderate crack depths. HY-100 structural steel is a very ductile high strength steel. The stress, strain and energy fields

along the curved crack front are determined for various loading conditions up to failure. Failure is determined by a local fracture criterion which uses strain energy density.Failure is defined as fracture initiation. Continuum material constitutive response which has been shown to be accurate at high strain levels is used to model the material response of HY-100 structural steel.

The two crack geometries considered are a semi-circle and a semi-ellipses with aspect ratios of 1.0 and 0.25, respectively. Crack depth ratios (a/t) considered are 0.25, 0.30 and 0.325. The surface cracks are embedded in a 254.0 mm wide and 25.4 mm thick plate of HY-100 structural steel. The surface cracked plates are independently subjected to tension or bending across the thickness. The global and local stress, strain and energy responses for the matrix of crack geometries presented are determined using finite element computational simulations. Critical strain energy density is used as the fracture parameter. The value of critical strain energy density used was previously determined from a series of round bar tensile specimens. Crack growth patterns based on the strain energy density profile along the crack perimeter are and a stress-strain history dependent critical strain energy density profile are determined.

Material Model and Fracture Criteria

An incremental rate independent plasticity theory available in the ABAQUS finite element program [25,26] was used for the material constitutive model. This standard model for plasticity is summarized here for completeness. Total strains in the multiaxial strain state ε_{ij} were obtained by the integration of the linearly decomposed rate of deformation tensor δ_{ij}. This integration was performed under the assumption that the elastic strains remain infinitesimal. The total multiaxial strain state ε_{ij}, expressed in terms of elastic and plastic components, is:

$$\varepsilon_{ij} = \varepsilon^{e}_{ij} + \varepsilon^{p}_{ij}$$

The total logarithmic uniaxial strain, ε, consistent with the integration of the rate of deformation tensor for a multiaxial strain state, is decomposed as:

$$\varepsilon = \varepsilon^e + \varepsilon^p$$

The yield function f takes the form:

$$f(\tau_{ij}) = \tau(\varepsilon^p)$$

where τ_{ij} and τ are the multiaxial Kirchoff (or Teffetz) and uniaxial stress states, respectively. The associated flow rule governs plastic strain increments by the relation:

$$d\varepsilon^p_{ij} = \lambda \frac{\partial f}{\partial \tau_{ij}}$$

In the case of purely elastic behavior (λ=0). For active material yielding (λ>0): Plastic strain increments also satisfied a dissipation equivalence condition:

$$\lambda = d\varepsilon^p \frac{\tau}{\tau_{ij} \frac{\partial f}{\partial \tau_{ij}}}$$

Plastic strain increments also must satisfy a dissipation equivalence condition:

$$\tau d\varepsilon^p = \tau_{ij} d\varepsilon_{ij}$$

and a consistency condition:

$$\frac{\partial f}{\partial \tau_{ij}} d\tau_{ij} - \frac{\partial \tau}{\partial \varepsilon^p} d\varepsilon^p = 0$$

The von Mises yield function is used and is:

$$f(\tau_{ij}) = \left(\frac{3}{2}(s_{ij}s_{ij})\right)^{1/2}$$

The deviatoric stress tensor s_{ij} is defined as:

$$s_{ij} = \tau_{ij} - \frac{1}{3}\tau_{kk}\delta_{ij}$$

where the hydrostatic component of stress is $\tau_{kk}/3$.

The Kirchoff stress and logarithmic strain measures are employed because of advantages gained in computational implementation. The Kirchoff stress tensor, τ_{ij}, is approximately equal to the more physically motivated Cauchy stress tensor, σ_{ij}, for deformations involving only small changes in values. This coincident is implicit in the current analysis. The uniaxial Cauchy stress - logarithmic strain constitutive response of the material were formally input, in multilinear form, as Cauchy stress and logarithmic strain pairs for the ABAQUS program. This constitutive formulation was determined in previous investigations by Matic, Father, Kirby and Jolles [27]. The accuracy with respect to both global and local response of the HY-100 constitutive response has been demonstrated by DeGiorgi, Kirby and Jolles [28].

The strain energy density per unit mass, w, of the material, is:

$$w = \lim_{\Delta V \to 0} \left(\frac{\Delta W}{\rho \Delta V}\right)$$

where W is the energy and V is volume. The terms of stress components, σ_{ij}, and strain components, ε_{ij}, and the mass density, ρ, the strain energy density is:

$$w = \int_0^{\varepsilon_{ij}} \frac{\sigma_{ij}}{\rho} d\varepsilon_{ij}$$

The strain energy density incorporates the contributions of both stress and strain quantities to the material history. The value of the energy density corresponding to local fracture of the material is:

$$w_c = \int_0^{(\varepsilon_{ij})_c} \frac{\sigma_{ij}}{\rho} d\varepsilon_{ij}$$

where w_c is the critical strain energy density value for a given stress-s train history. The value of w_c is generally path dependent, although a representative value may be practical for engineering applications.

For ductile metals, the mass density values only slightly, even over large ranges of deformations. For this reason, it is possible to define an energy per unit volume density:

$$w = \lim_{\Delta V \to 0} \frac{\Delta W}{\Delta V}$$

or

$$w = \int_0^{\varepsilon_{ij}} \sigma_{ij} de_{ij}$$

with an associated critical value:

$$w_c = \int_0^{(\varepsilon_{ij})_c} \sigma_{ij} de_{ij}$$

The energy per unit mass is a fundamental quantity however, the energy per unit volume is equally appropriate for use with constant volume deformation processes.

For the case of a uniaxial representation of true stress versus true strain material response, the critical energy density corresponds to the area under the uniaxial stress-strain curve:

$$w = \int_0^{\varepsilon_c} \sigma d\varepsilon$$

This representation is suitable for use with traditional constitutive formulations which rely on uniaxial stress-strain data for material response characterization.

For a multiaxial state of stress, each of the six stress-strain pairs, three normal and three shear, must be evaluated and summed. It should be noted that one or more individual terms, but not all six terms, in the muliaxial expression can be negative. The total, w_c, must be positive.

Prediction of fracture inititaion employing a local criterion requires the identification of local maximum energy densities and comparison of these maxima with a local critical energy density value. For a materially inhomogeneous component, the maximum local energy densities in each constituent material must be identified and compared with the corresponding local fracture toughness value. For a material homogeneous component, as considered in the current investigation, one critical energy density value is used to characterize local fracture resistance. The maximum local energy density must be identified at each increment of loading and compared to the critical values.

The location of the energy density maxima may vary during the loading history. Additional deformation can be sustained without fracture as long as:

$$w < w_c$$

Local fracture coincides with the energy density attaining the critical energy density value for the material at some point:

$$w = w_c$$

The critical energy density value used in this investigation, as obtained from the constitutive characterizing previously referenced, reflect the multiaxial history dependence of w_c.

Surface Crack Plate Model

Two surface crack geometries were modeled using the finite element method. The surface crack geometries considered are a semi-elliptical cracks with aspect ratios of 1.0 and 0.25. The two crack profiles modeled are shown in Figure 3. The surface crack is embedded in a flat plate of dimensions 254.0 mm wide by 25.4 mm thick. The plate is sufficiently long so that there are minimal end constraint effects on the model. Three crack depths are considered for each crack geometry: 0.25, 0.30 and 0.325. The finite element models are constructed so that only one model is needed for each crack geometry.

The finite element program ABAQUS [25] is used for the computational simulations. The two basic finite element models are shown in Figures 4 through 7. Specimen, crack profile and loading condition symmetry required only one quarter of the specimen to be modeled. The initial crack faces lie along the axis of symmetry.

Type C3D8 elements were used in the model. These are continuum three-dimensional brick elements with 8 nodes defining the element vertices. Sufficient mesh refinement allows for accurate modeling using these linear displacement interpolation elements. No crack tip singularity is included in the model.

All analyses used full geometric nonlinearity to account for large strains and large rotations. An updated Lagrangian formulation was used for incremental solution in ABAQUS. A modified Rik's algorithm which is both load and displacement controlled is used to allow for unloading. Use of the

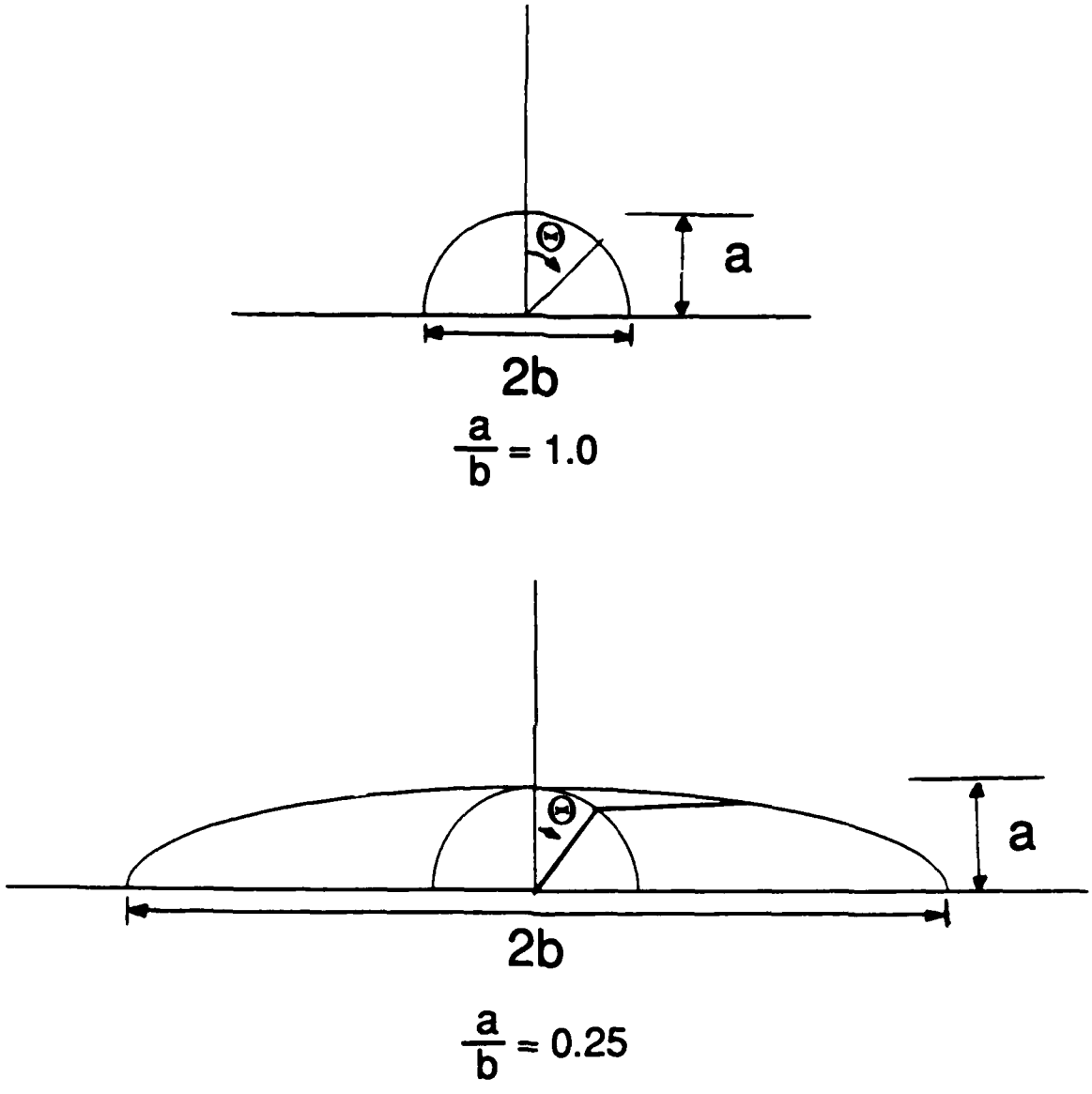

Fig. 3 — Semi-Circular (a/b = 1.0) and Semi-Elliptical (a/b = 0.25) Surface Crack Geometries

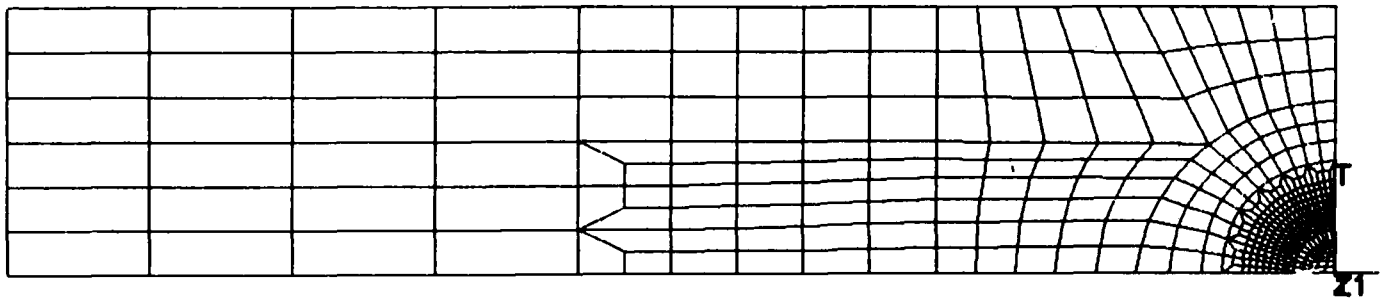

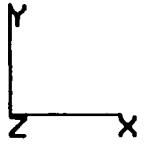

INTERFACE? 1.NEUTRAL 2.NASTRAN 3.ANSYS 4.ABAQUS 5.SINDA
6.ADINA 7.IGES 8.CS/NASTRAN 9.MORE 10.END
>

Fig. 4 — Semi-Circular (a/b = 1.0) Surface Crack Finite Element Model: x-y Plane Pattern

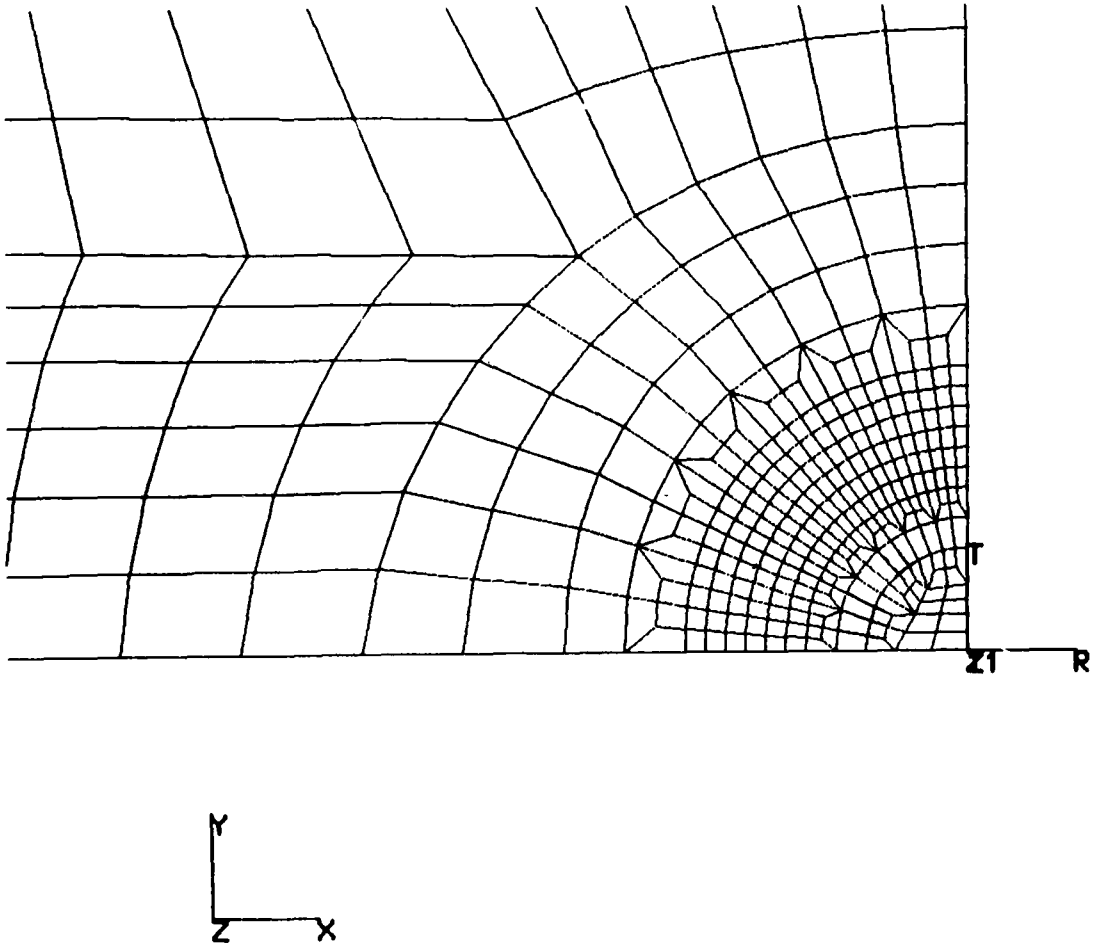

INTERFACE? 1.NEUTRAL 2.NASTRAN 3.ANSYS 4.ABAQUS 5.SINDA
6.ADINA 7.IGES 8.CS/NASTRAN 9.MORE 10.END
>

Fig. 5 — Semi-Circular (a/b = 1.0) Surface Crack Finite Element Model; Close Up of Surface Crack Region

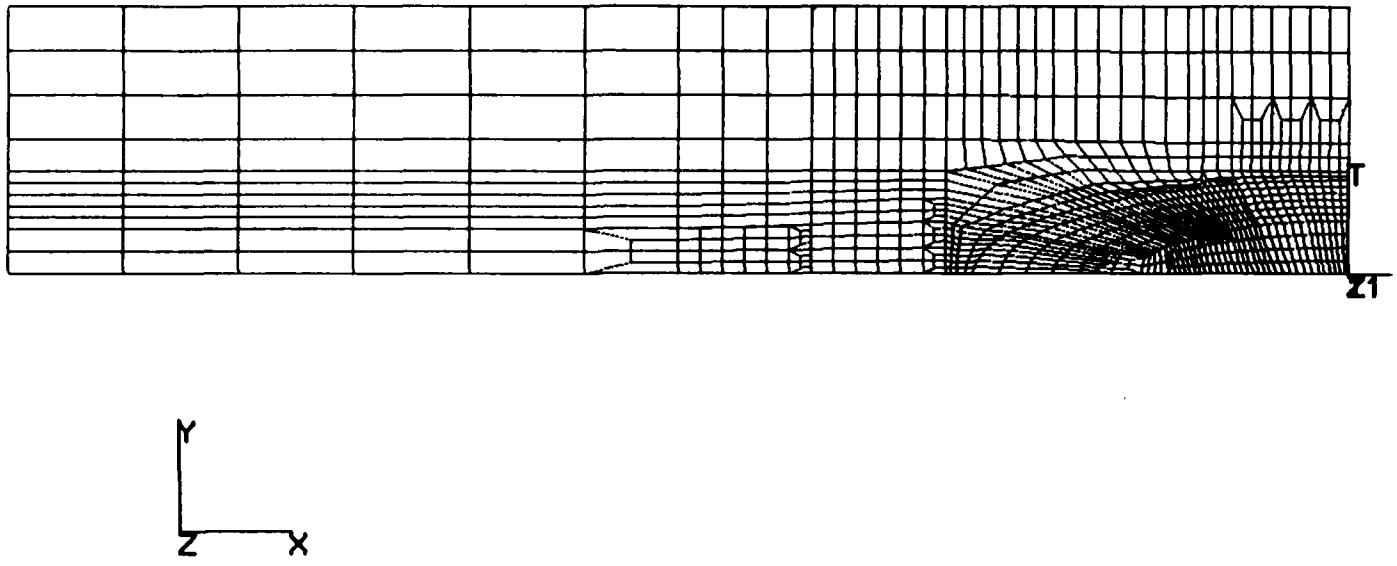

INTERFACE? 1.NEUTRAL 2.NASTRAN 3.ANSYS 4.ABAQUS 5.SINDA
6.ADINA 7.IGES 8.CS/NASTRAN 9.MORE 10.END
>

Fig. 6 — Semi-Elliptical (a/b = 0.25) Surface Crack Finite Element Model; x-y Plane Pattern

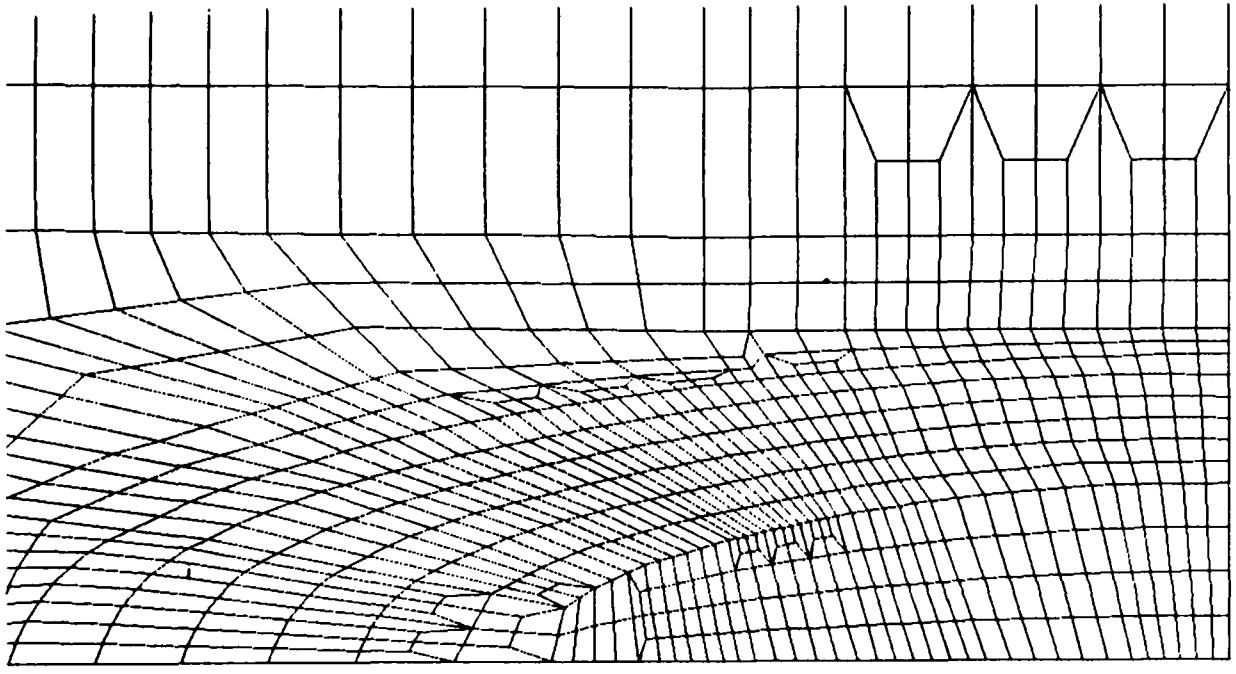

INTERFACE? 1.NEUTRAL 2.NASTRAN 3.ANSYS 4.ABAQUS 5.SINDA
6.ADINA 7.IGES 8.CS/NASTRAN 9.MORE 10.END
>

Fig. 7 — Semi-Elliptical (a/b = 0.25) Surface Crack Finite Element Model; Close Up of Surface Crack Region

modified Rik's algorithm also enhances the numerical stability of the solution procedure.

The finite element model for the surface crack of aspect ratio 1.0 is shown in Figures 4 and 5. The model consists of 3400 elements and 4176 nodes which result in 12528 total variables within the model. There are 25 nodes and 24 elements along the crack front as shown in Figure 6. The crack front is moved radially outward maintaining the aspect ratio of 1.0 for the different crack lengths. The finite element model was generated using the interactive mesh generating capability of PATRAN [29]. The mesh was optimized using PATRAN prior to conversion to an ABAQUS input deck. The maximum D.O.F. wavefront as optimized by PATRAN is 882.

The finite element model for the surface crack of aspect ratio 0.25 is shown in Figures 6 and 7. The model consists of 3756 elements and 5085 nodes. Multi-point constraints, a option with ABAQUS to constrain nodes to prescribed displacement or to displacements based on nodal displacements to be determined as part of the solution, were used as a modeling aid in this mesh. The total number of variables in the model is 15255. There are 52 nodes and 51 elements along the crack tip perimeter. The crack front is moved radially outward maintaining an aspect ratio of 0.25 for all crack depths. The mesh was created with the program PATRAN. The finite element mesh was optimized using PATRAN and the maximum D.O. F. wavefront was 594.

Remote tension was approximated on both models by constraining nodes along the plane of the crack in the perpendicular direction and applying a uniform displacement in the perpendicular direction at the far end of the model (Figure 8).

Bending across the thickness was modeled as four point bending as shown schematic in Figure 8. Nodal constraints were applied along the line of nodes representing the support. Uniform nodal displacements were applied to the line of nodes corresponding to the load point. Symmetry conditions were applied at the crack plane.

In both loading conditions the load was incrementally increased until the maximum strain energy density along the crack front equalled or exceeded the material critical strain energy value.

Results

The results of the surface crack simulations are presented as global and local material responses.

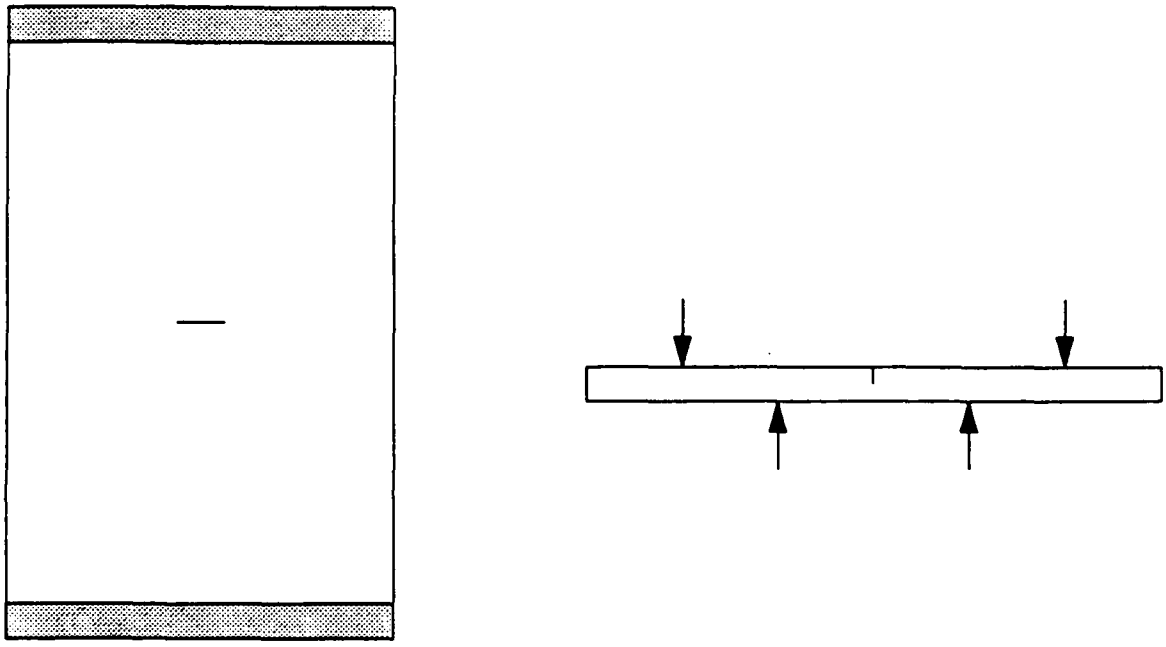

Fig. 8 — Schematic of Applied Loading to Finite Element Model

The global load displacement response for the matrix of crack geometries examined are shown in Figures 9 through 15. Nominal stress is the remote tension stress applied or the maximum bending stress applied assuming no crack. The reported value of CMOD is the displacement measured at the center of the front profile of the surface crack. This point is identified as "CL" in Figure 1. In all cases, the plates containing the surface flaw were loaded until the critical strain energy density value was reached at some point along the crack perimeter.

Unloading is observed for the semi-circular crack at all depths when subjected to remote tension loading. No unloading is observed for semi-circular cracks subjected to bending. Unloading under applied tension is observed for only the deepest semi-elliptical crack. No unloading is observed for semi-elliptical cracks subjected to bending.

A comparison of all global responses for tension loading is shown in Figure 15. All remote tension loadings, regardless of the crack geometry or depth, result in almost identical global load displacement responses.

In contrast, bending loads result maximum nominal stresses which are below the yield strength for all crack geometries. The global load displacement curves for all crack geometries subjected to bending are also shown in Figure 15. The global load displacement responses can be readily divided into two distinct geometrically dependent responses. The global response is more sensitive to crack size when the plate is subjected to bending loads than when the plate is subjected to tension loads.

Local material response is represented by the strain energy density profile along the curved crack perimeter. The strain energy density profiles along the crack perimeter for various load levels are shown in Figure 16 for the semi-circular crack (a/b=1.0) subjected to tension and with increasing crack depths of 0.25, 0.30 and 0.325. The maximum strain energy density occurs at the free surface. This is similar to LEFM results [14,18].

The strain energy density profiles for the semi-circular crack subjected to bending are shown in Figure 17 for crack depths of 0.25, 0.30 and 0.325, respectively. The maximum strain energy density occurs at the free surface similar to LEFM results [14,18].

The consistency between fracture critical profiles for the range of crack depths examined subjected to tension or bending is shown in Figure 18. A comparison of the criticality of fracture parameters between the current continuum constitutive response analysis and LEFM analysis for similar crack geometries are shown in Figure 19. The nonlinear material constitutive

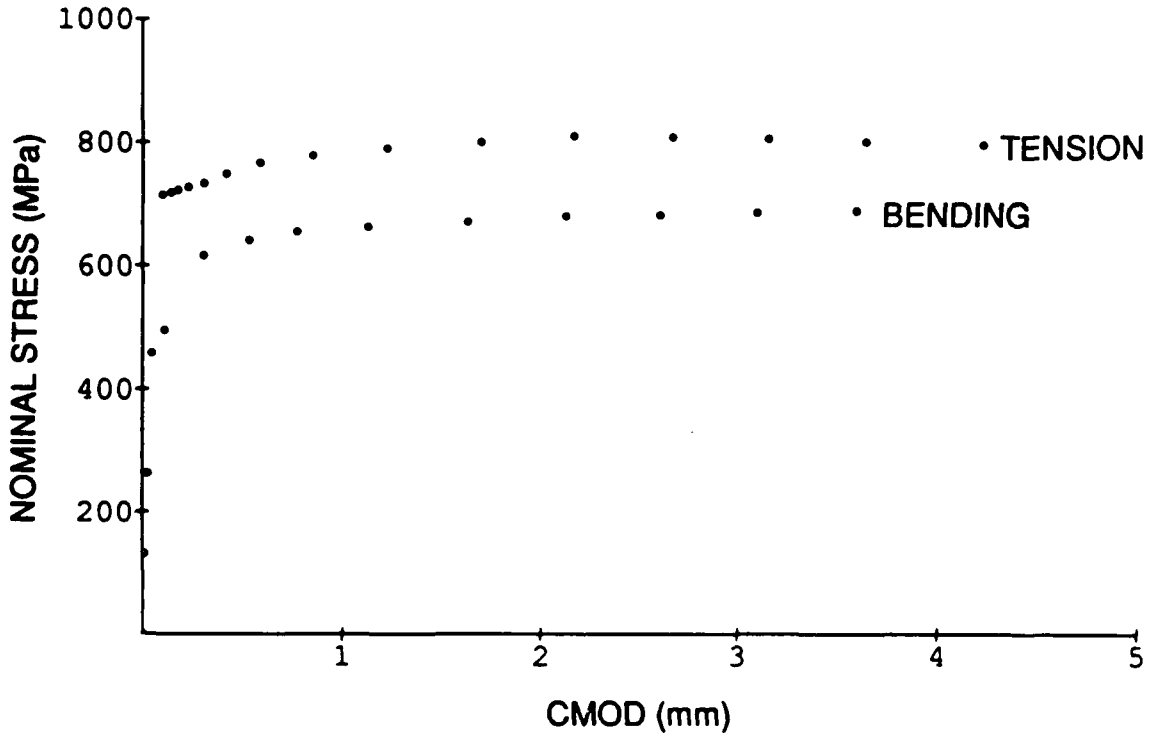

Fig. 9 — Global Nominal Stress — CMOD Response for Semi-Circular (a/b = 1.0) Crack with a/t = 0.25

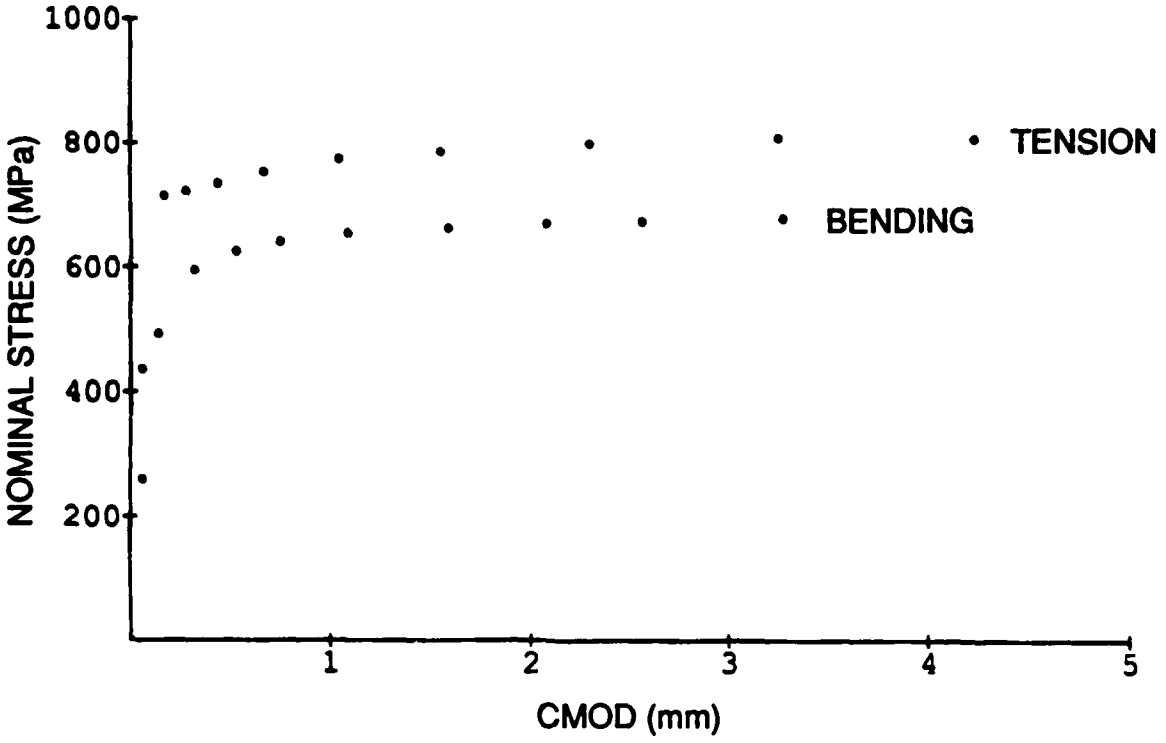

Fig. 10 — Global Nominal Stress — CMOD Response for Semi-Circular (a/b = 1.0) Crack with a/t = 0.30

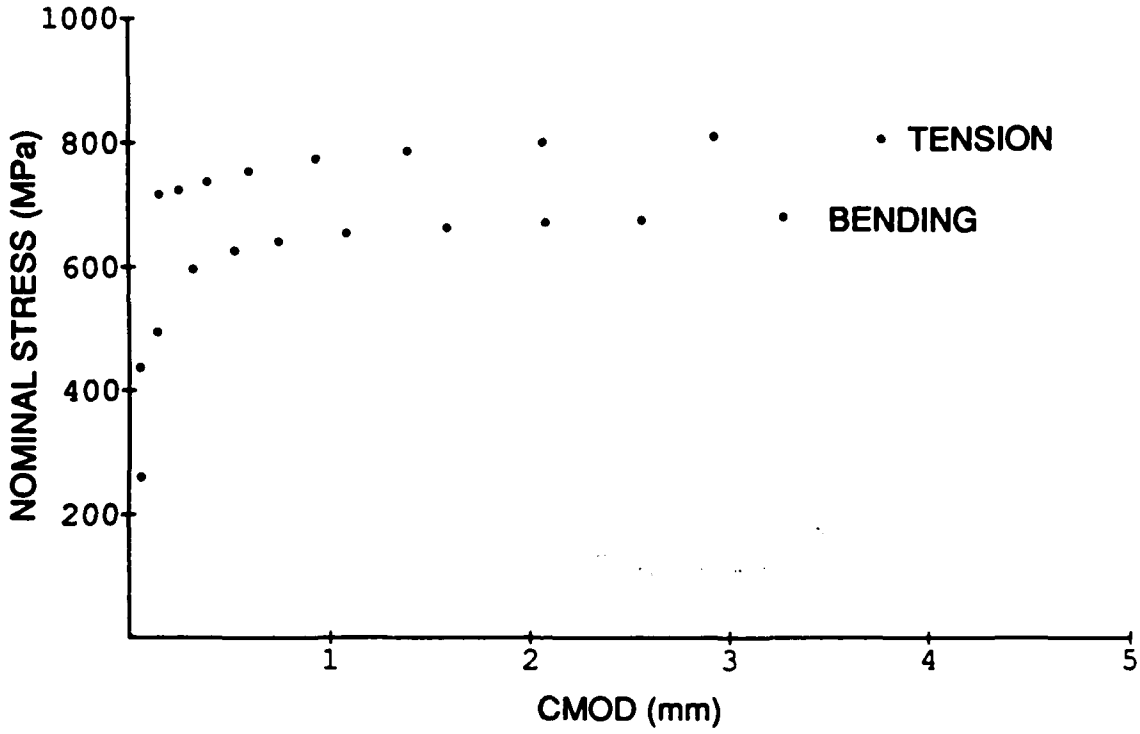

Fig. 11 — Global Nominal Stress — CMOD Response for Semi-Circular (a/b = 1.0) Crack with a/t = 0.325

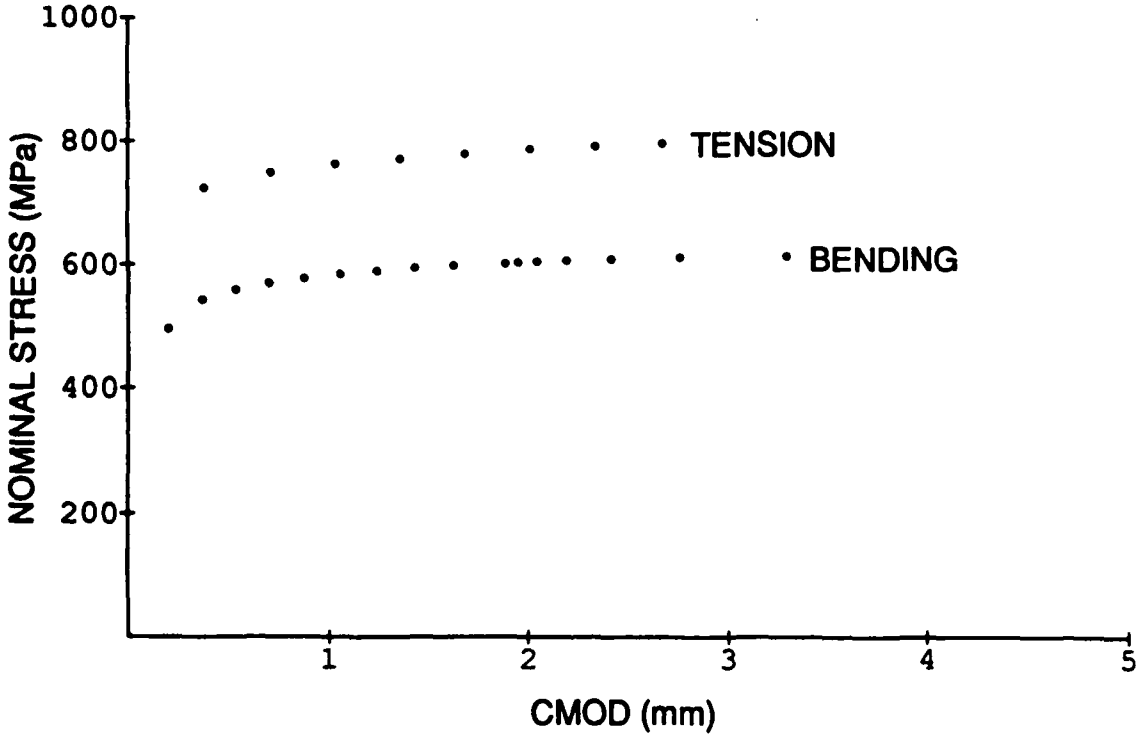

Fig. 12 — Global Nominal Stress — CMOD Response for Semi-Elliptical (a/b = 0.25) Crack with a/t = 0.25

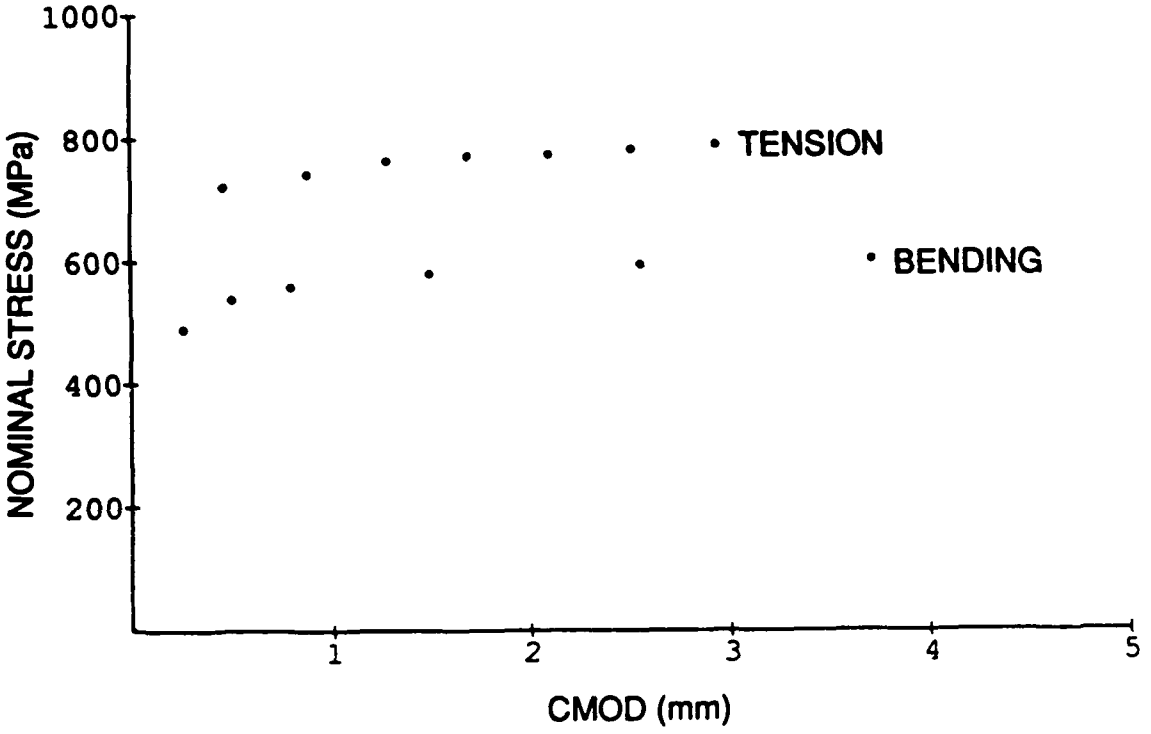

Fig. 13 — Global Nominal Stress — CMOD Response for Semi-Elliptical (a/b = 0.25) Crack with a/t = 0.30

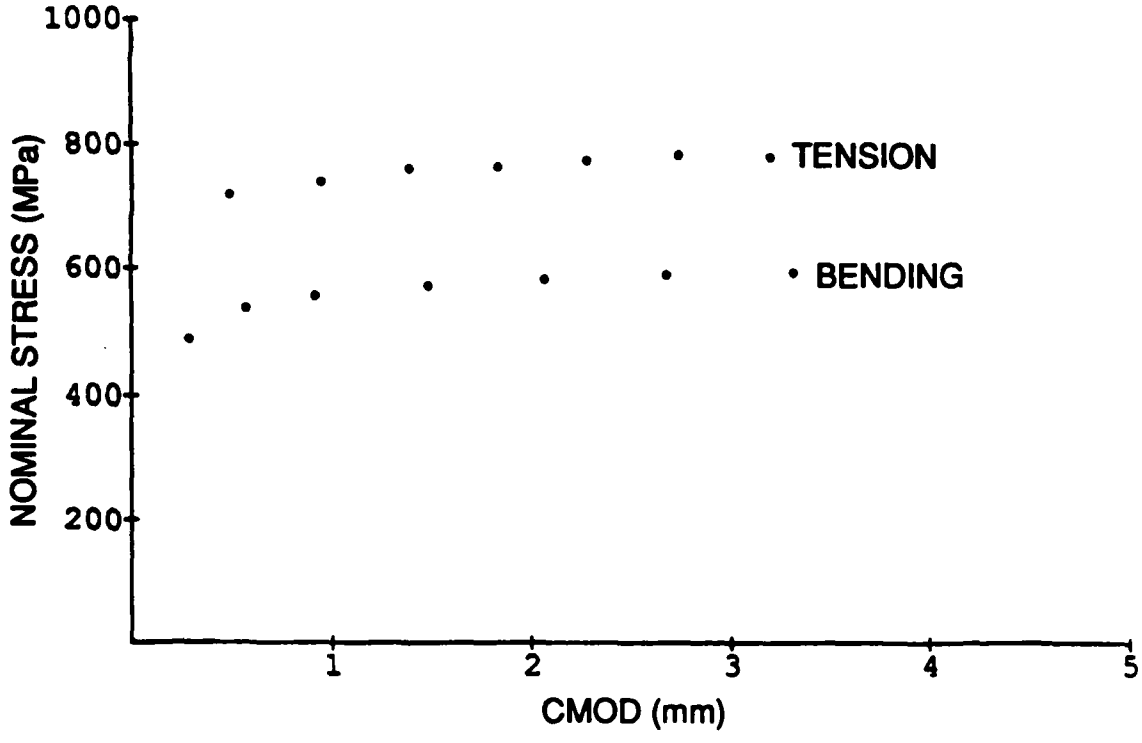

Fig. 14 — Global Nominal Stress — CMOD Response for Semi-Elliptical (a/b = 0.25) Crack with a/t = 0.325

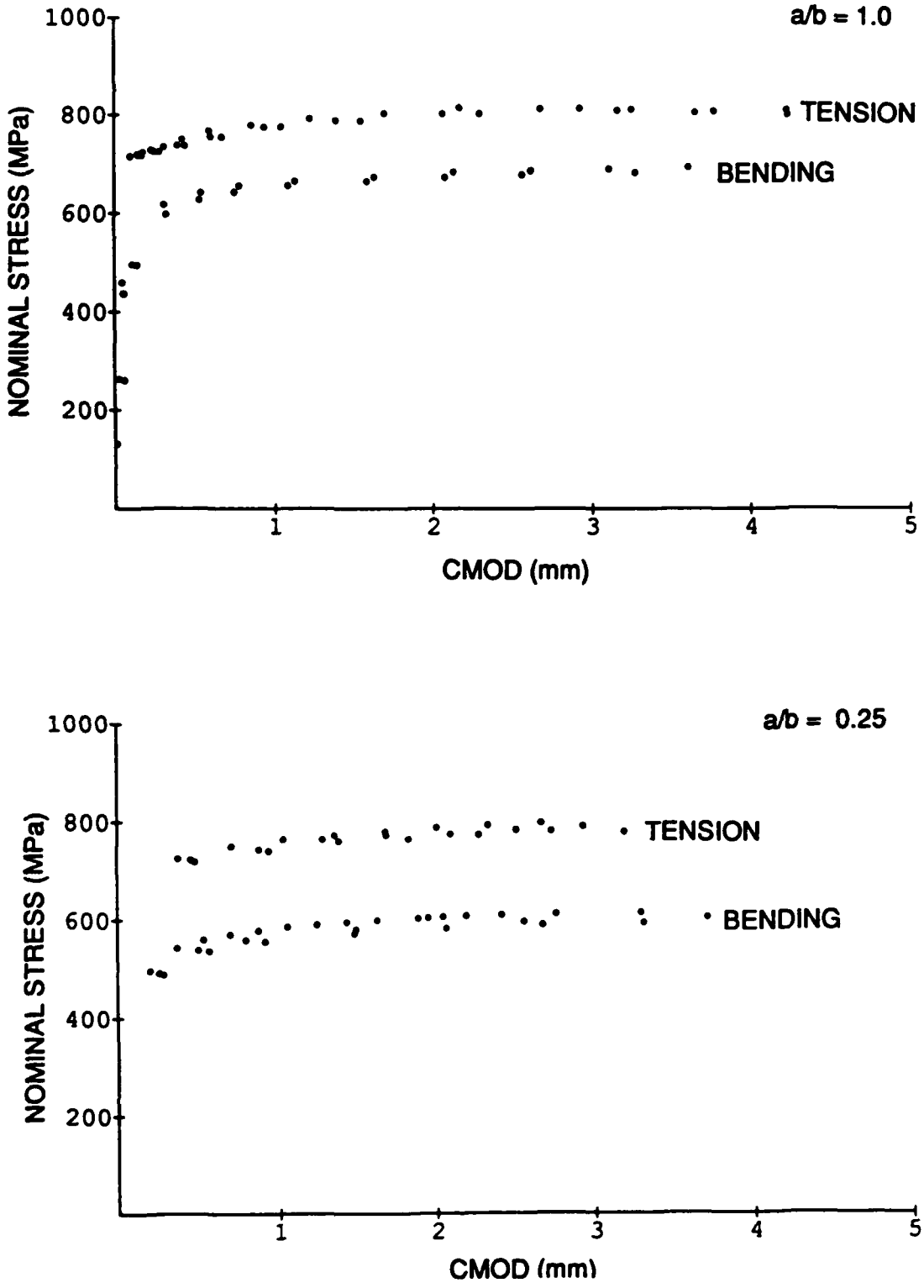

Fig. 15 — Global Nominal Stress — CMOD Response for Semi-Circular (a/b = 1.0) Semi-Elliptical (a/b = 0.25) Cracks

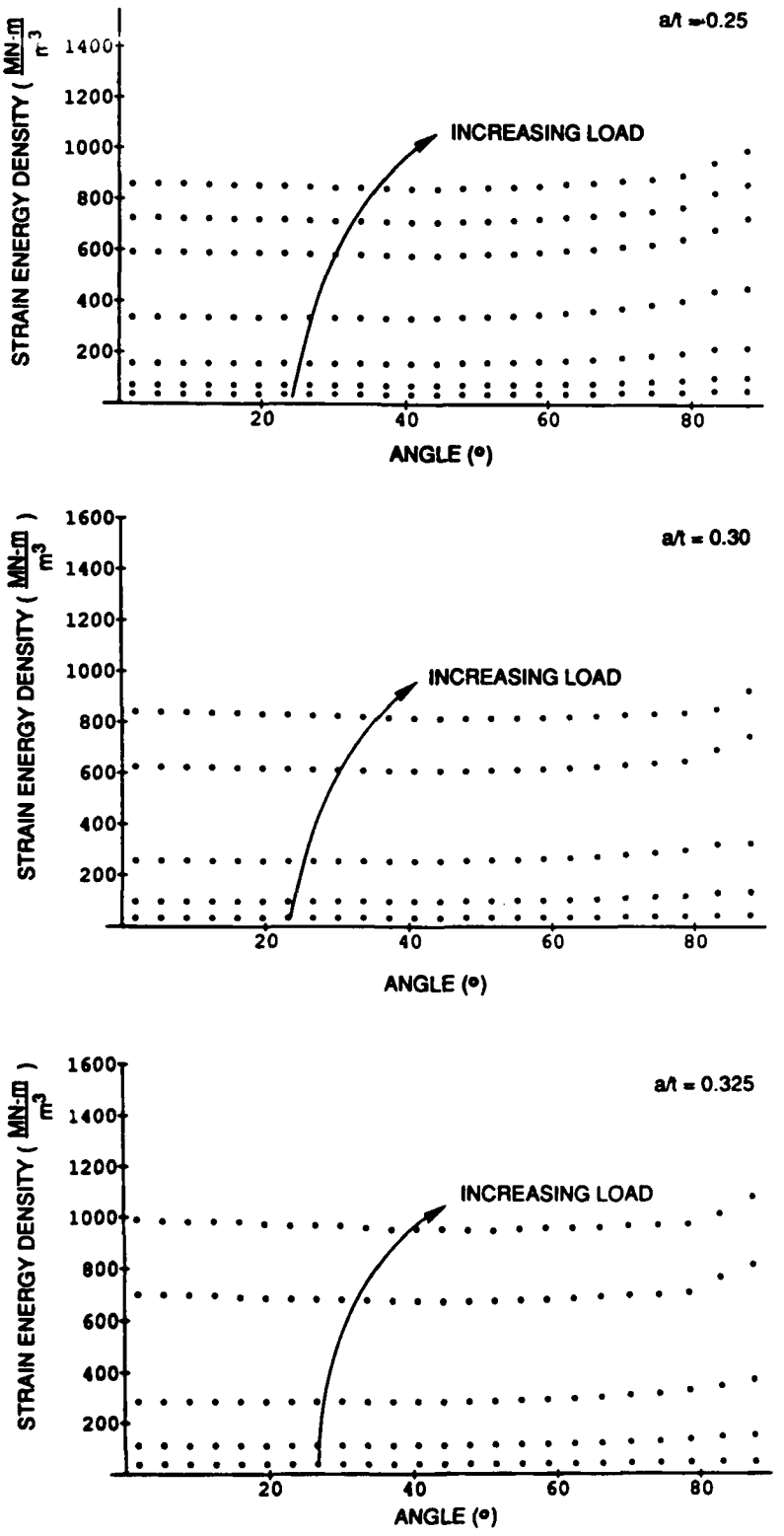

Fig. 16 — Strain Energy Density Profiles for Semi-Circular (a/b = 1.0) Cracks In Tension

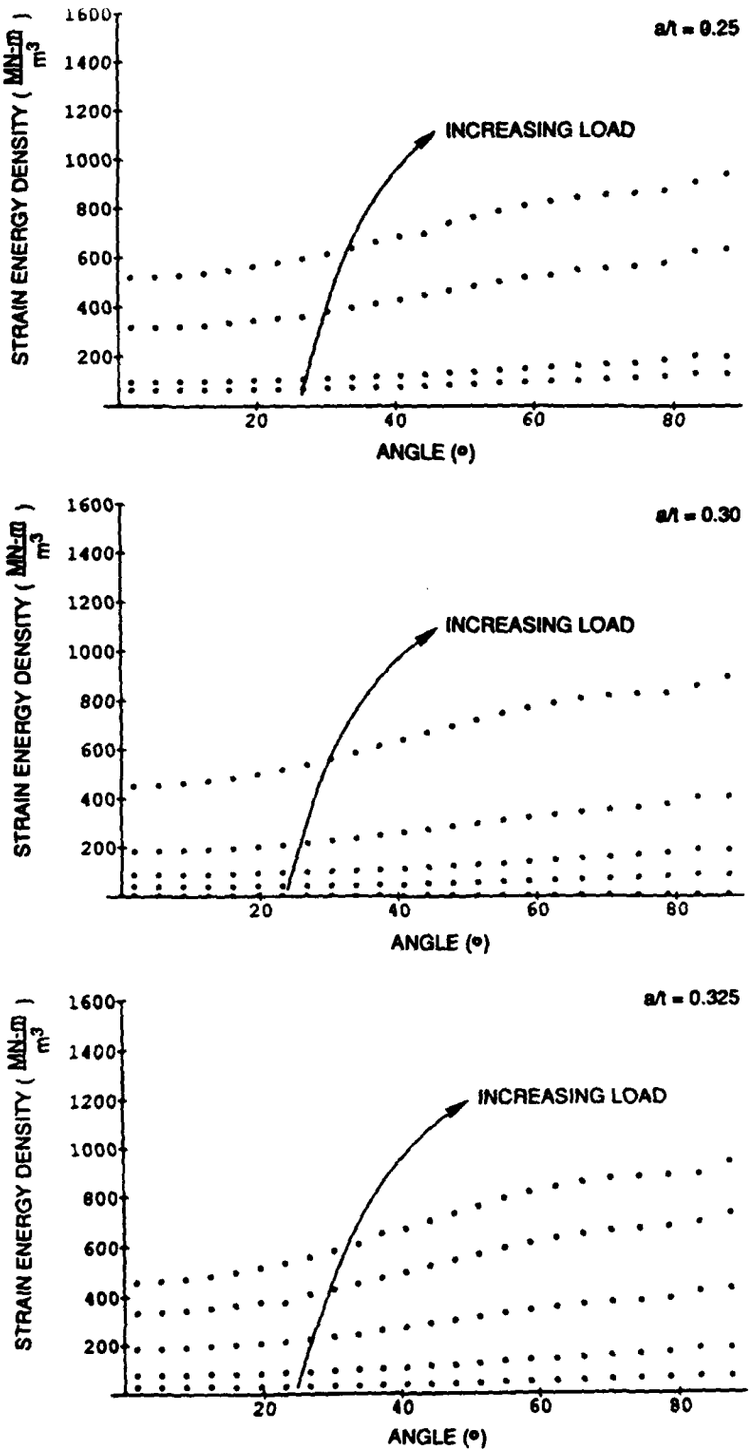

Fig. 17 — Strain Energy Density Profiles for Semi-Circular (a/b = 1.0) Cracks In Bending

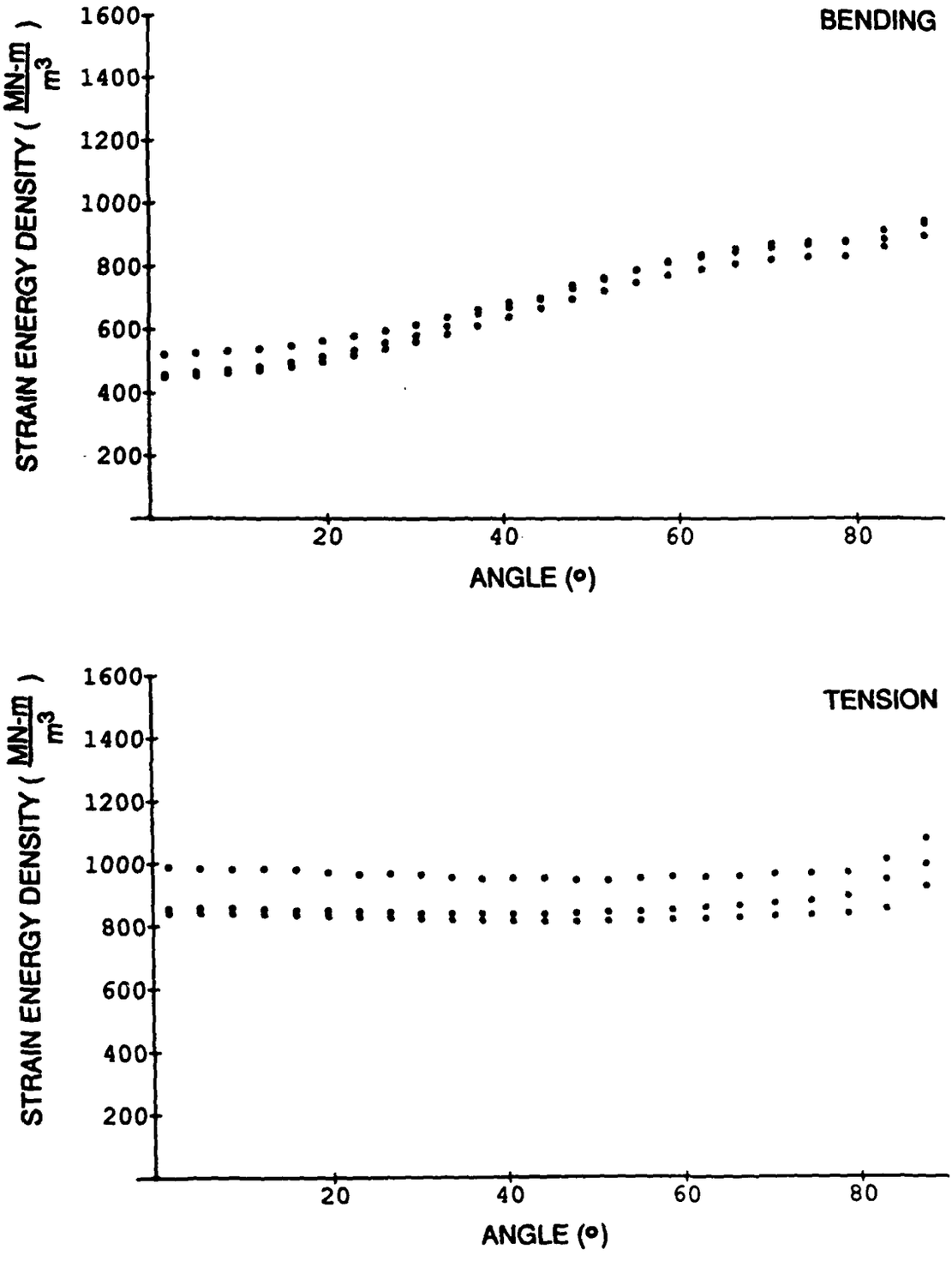

Fig. 18 — Critical Strain Energy Density Profiles for Semi-Circular Cracks (a/b = 1.0)

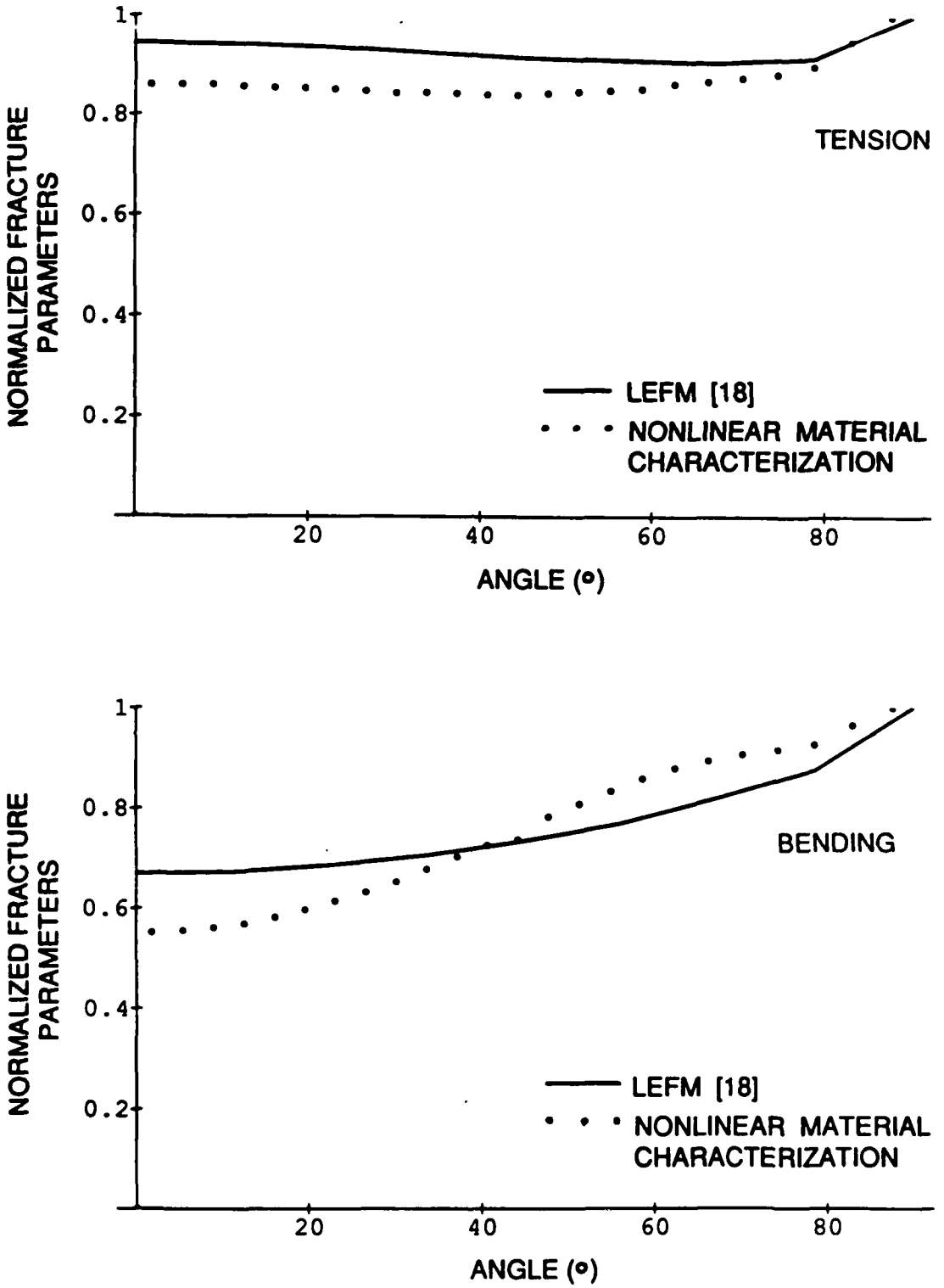

Fig. 19 — Comparison of Normalized Strain Energy Density Response and LEFM Profiles for Semi-Circular (a/b = 1.0) Cracks

response results in a flatter strain energy profile than may be expected by simple extrapolation of LEFM results.

When the semi-circular crack is subjected to bending across the thickness there is a region along the crack perimeter bounded 45° and 80° where there is a localized increase in the strain energy density. There is no similar feature on LEFM predicted fracture criteria curves.

Typical tension and bending strain energy density profiles at fracture initiation are shown in Figure 20. Even though the maximum strain energy density occurs at the same location, the profiles are not similar.

The strain energy density profiles for various stages of tension loading for the semi-elliptical crack (a/b=0.25) at depths of 0.25, 0.3 and 0.325 are shown in Figures 21. The maximum strain energy density occurs at the crack center. The location of maximum fracture criteria value is similar to LEFM results [14,18].

The strain energy density profiles for the semi-elliptical crack subjected bending are shown in Figures 22 for crack depths of 0.25,0.30 and 0.325. The maximum strain energy density occurs at the crack center, similar to LEFM fracture criteria results [14,18].

The consistency between fracture critical curves for the crack depths examined subjected to tension or bending can be seen in Figure 24. Local minimums in the region bounded by angular measurements of 70° and 90° for a crack depth of 0.25 are due to element geometry in this region. The greater crack depths have a more uniform mesh pattern and this region of the strain energy density profile smooths in consequence. There is good agreement in the strain energy density profiles when different crack depths are compared, as shown in Figure 23, despite the individual element geometries along this one region.

A comparison of fracture parameter criticality between the continuum constitutive response analysis and LEFM results for similar crack geometries are shown in Figure 24. For both tension and bending applied loadings, the nonlinear constitutive response analysis results shown a greater difference in fracture perimeter between the crack center and the free surface point. In the case of tension loading the difference in strain energy density at the extreme points of the surface crack is greater than that reported for J values [15] for a deeper semi-elliptical crack of different geometry.

Typical tension and bending strain energy density profiles at fracture initiation are shown in Figure 25. The maximum strain energy density occurs at the same location and the profiles are similar.

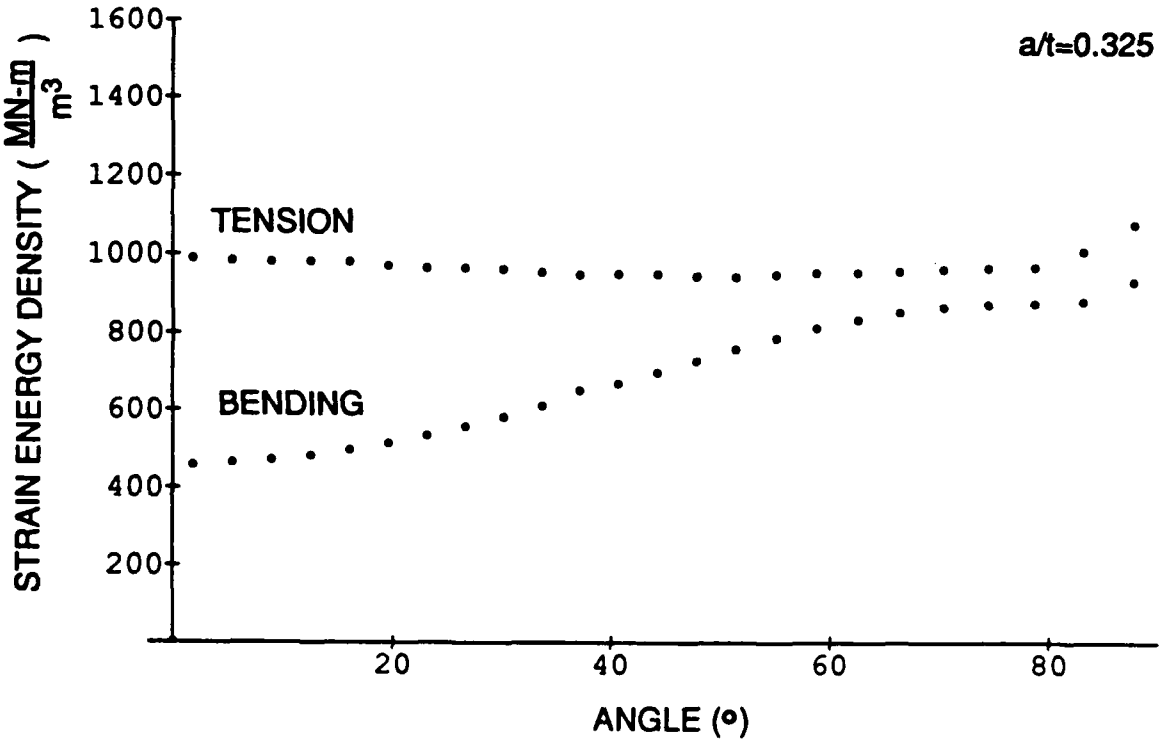

Fig. 20 — Comparison of Critical Strain Energy Density Profiles In Tension and Bending for Semi-Circular (a/b = 1.0) Cracks

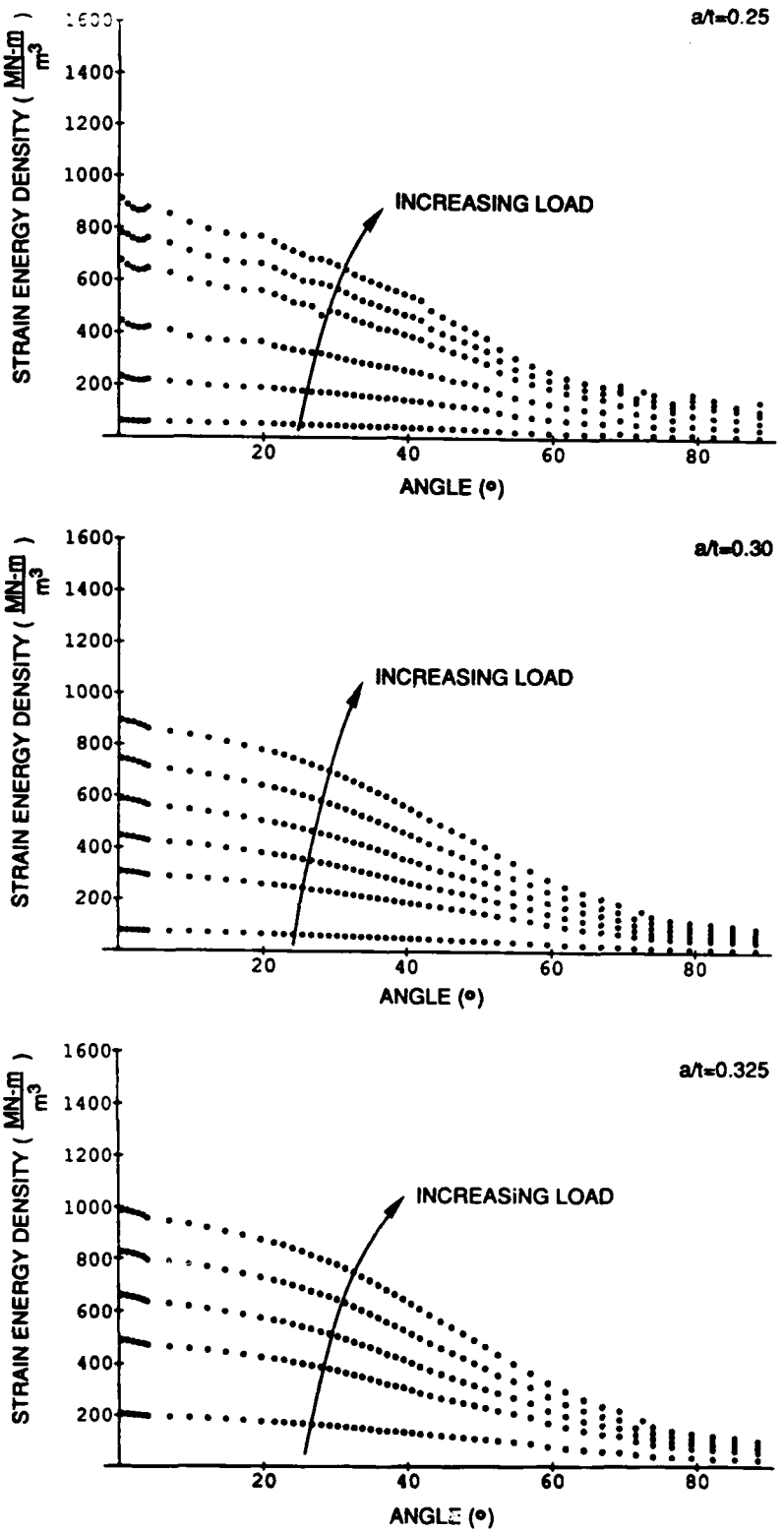

Fig. 21 — Strain Energy Density Profiles for Semi-Elliptical (a/b = 0.25) Cracks In Tension

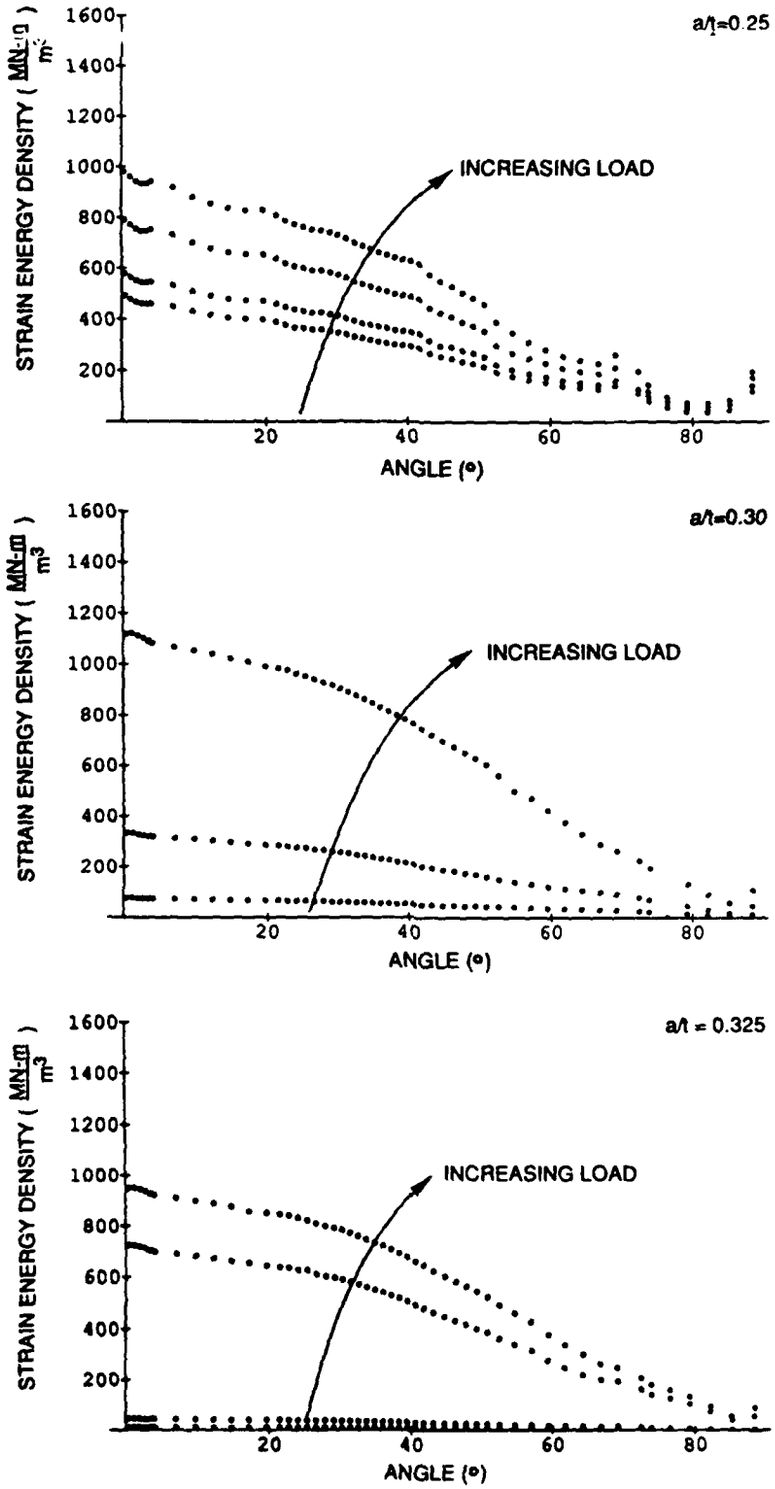

Fig. 22 — Strain Energy Density Profiles for Semi-Elliptical (a/b = 0.25) Cracks In Bending

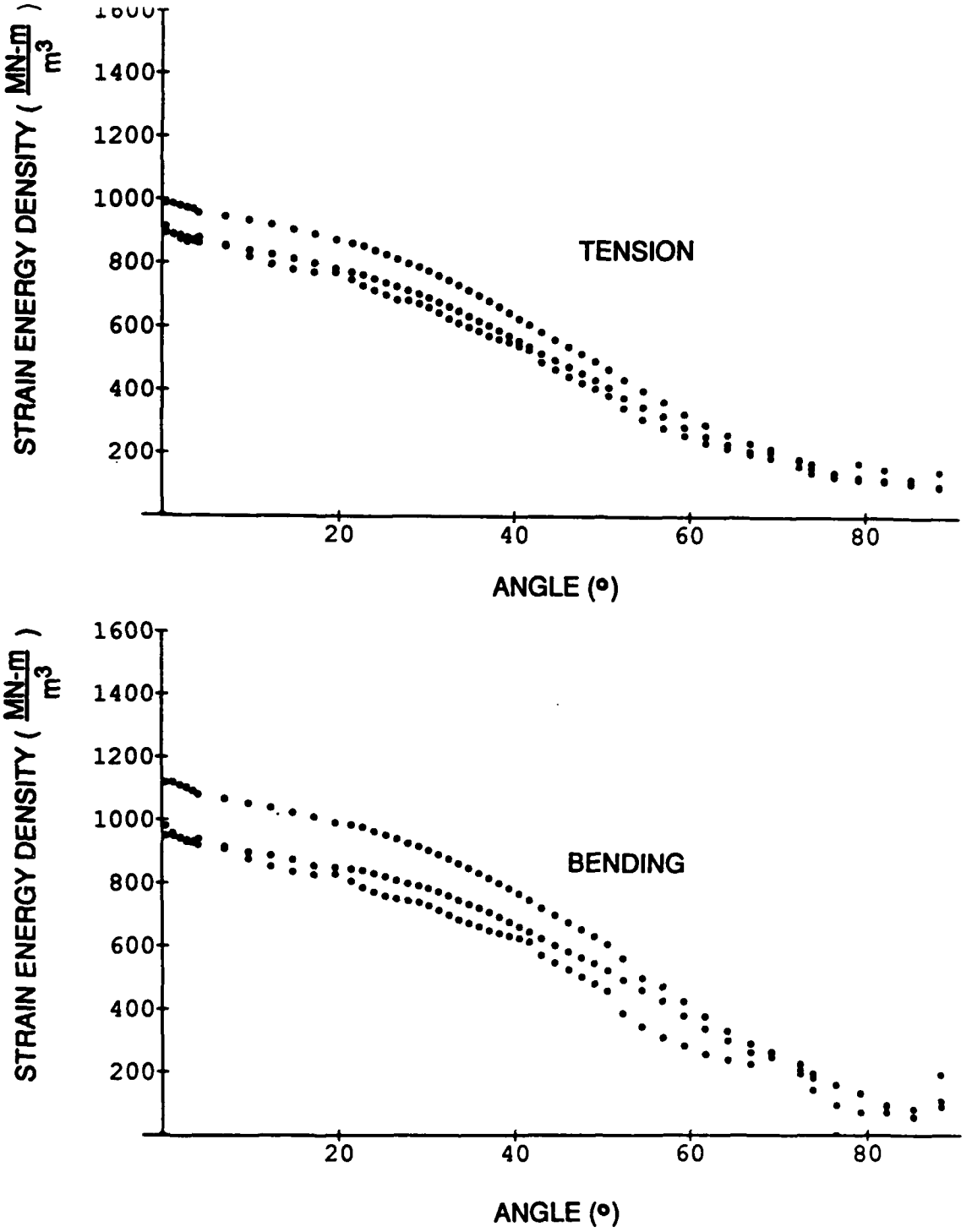

Fig. 23 — Critical Strain Energy Density Profiles for Semi-Elliptical (a/b = 0.25) Cracks

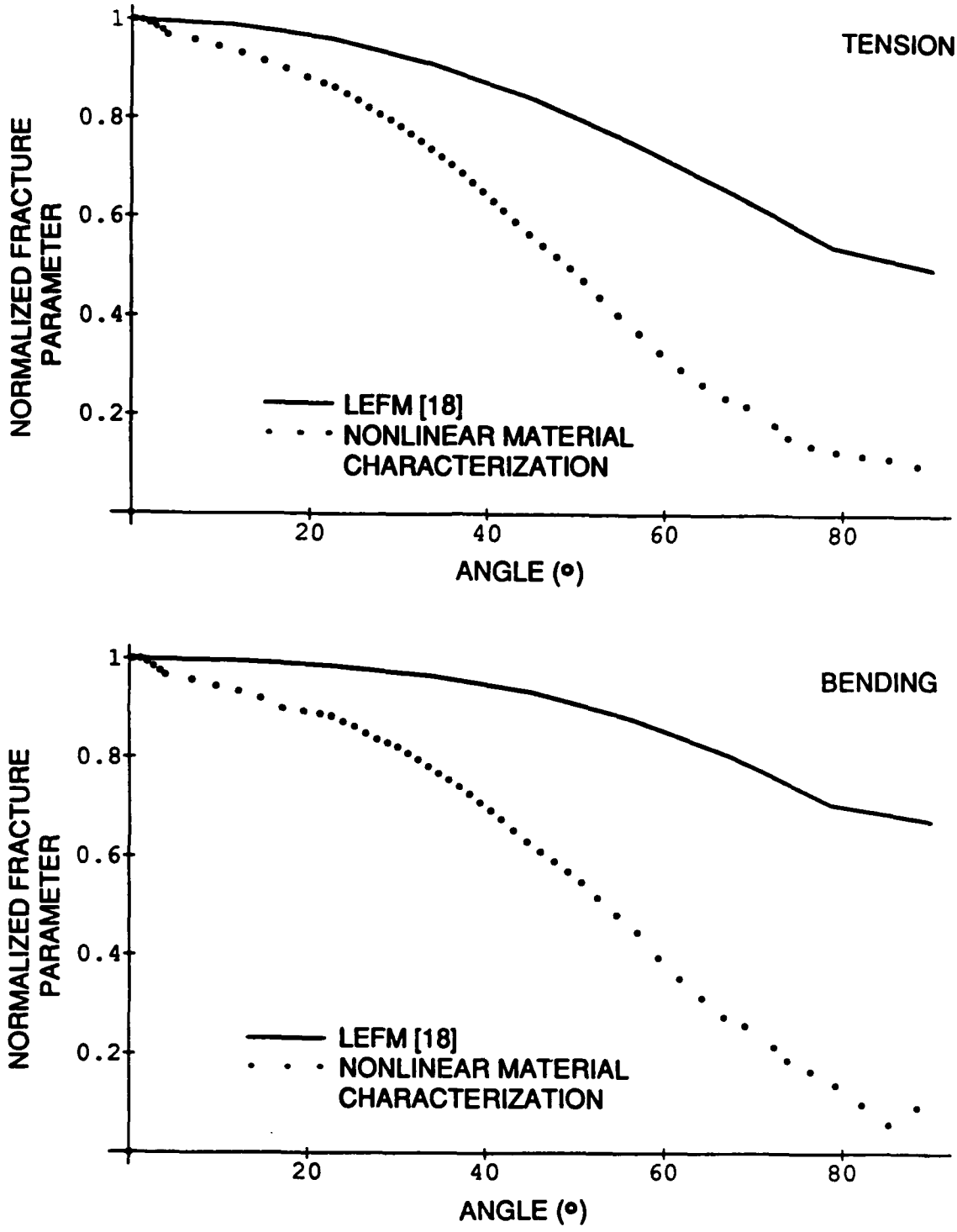

Fig. 24 — Comparison of Normalized Strain Energy Density Response and LEFM Profiles for Semi-Elliptical (a/b = 0.25) Cracks

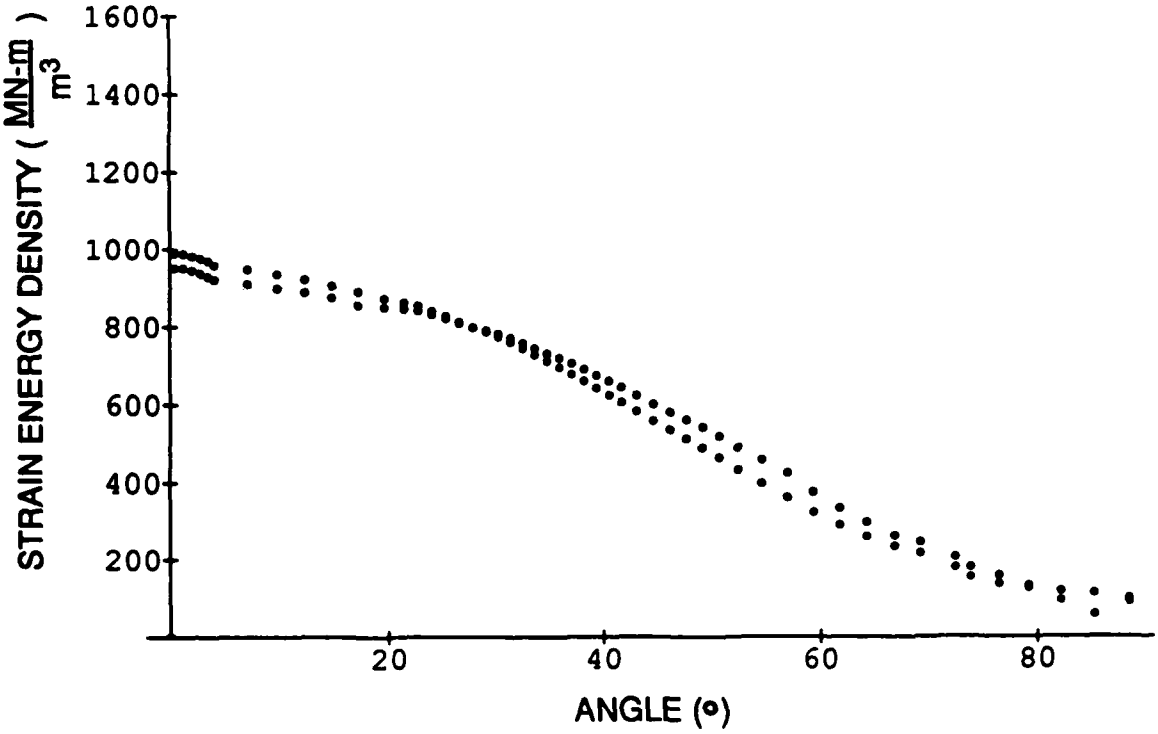

Fig. 25 — Comparison of Critical Strain Energy Density Profiles In Tension and Bending for Semi-Elliptical (a/b = 0.25) Cracks

Fracture Criterion Variation Due to Constraint

In the preceding interpretation of results, it was assumed that the critical strain energy density is a constant value independent stress-strain history. It is know that the critical strain energy density as determined from round bar tensile specimens is dependent on the constraint state [27]. Thick short tensile specimens which simulate plane strain conditions have a lower critical strain energy density value than long thin specimens which are representative of plane stress conditions. The degree of constraint will vary along the curved crack perimeter from near plane strain to plane stress at the free surface. Inclusion of the known variation of the local fracture parameter in the criticality evaluation is required for an accurate representation of local fracture initiation response.

In order to estalish a critical strain energy density profile, the extent of nearly plane strain conditions along the curved crack perimeter must be determined. In the current analysis, the extend of plane strain conditions is estimated from the analytical evaluations and compared with previous estimates of the extend of plane strain conditions. Francis and Davidson [30] experimentally measured plastic zones by electrolytic etching studies on Fe-3Si specimens containing surface flaws of varying geometries. It was determined from this study that nearly plane strain conditions exist for the crack front between 0 and at least 45^{o}. Analytical work by Gangming and Yongyuan [17] indicates that plane strain conditions exist until at least 65^{o} along the crack perimeter. Their determination of the extent of plane strain conditions is based on the convergence characteristics of the boundary element numerical simulation performed. Trantina et al [21] estimated based on stress component ratios that plane strain conditions exist until approximately 75^{o} along the crack perimeter.

In the current analysis, the ratio of maximum to minimum principle stress is used as a measure of the constraint state. Typical variation in principle stress components ahead of the crack tip for the two crack geometries studied in the current work are shown in Figure 26. The principle stress ratio indicates the transition from plane strain conditions occurs at approximately 60^{o} along the crack perimeter for both crack geometries. This is consistent with the previous mentioned work [17,21,30].

The critical strain energy density for HY-100 structural steel has been determined from a series of round bar tensile tests and numerical simulations [27]. The critical strain energy density for plane strain conditions is 889.0 MN-m/m^3 (1.29 x10^5 in-lb/in^2). The critical strain energy density value

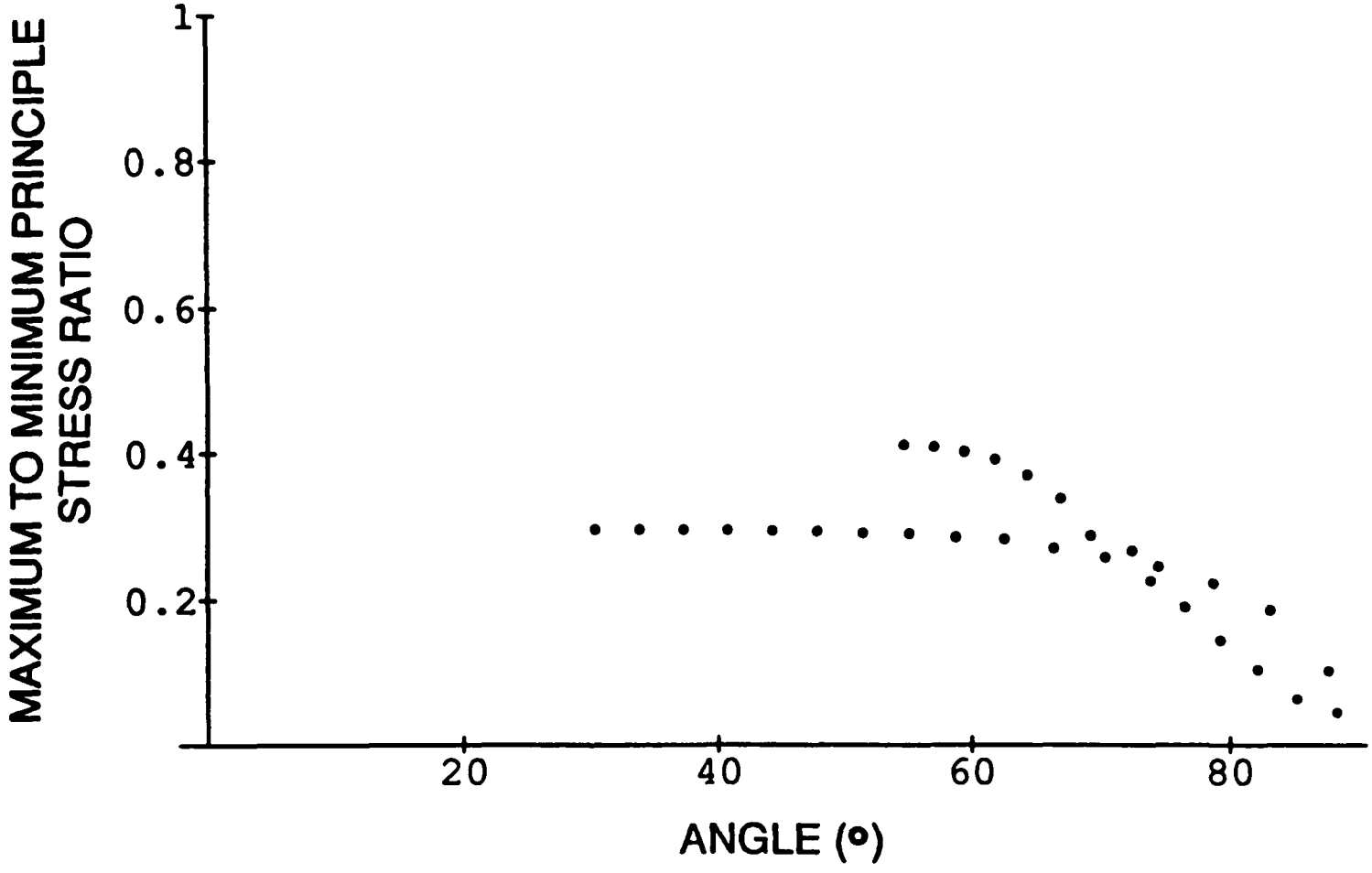

Fig. 26 — Ratio of Minimum to Maximum Principle Stress for Semi-Circular (a/b = 1.0) and Semi-Elliptical (a/b = 0.25) Cracks In Tension

representative of plane stress conditions is 1394.0 MN-m/m^3 (1.92 x10^5 in-lb/in^2) [27]. A simple bi-linear failure curve is created based on the results shown in Figure 26 and the critical strain energy density values for plane strain and plane stress conditions. Typical strain energy density profiles for each of the crack geometries and loading conditions studied are compared to the failure curve.

The strain energy density profile for the semi-circular (a/b=1.0) crack subjected to tension loading is compared to the critical strain energy density curve in Figure 27. Even though the maximum strain energy density occurs at the free surface where plane stress conditions occur, fracture initiation occurs at 0°, the crack center.The relatively flat nature of the strain energy density curve will result in crack growth along the perimeter from the crack center to approximately 60°. The strain energy density profile in this region indicates that there will be a slightly greater amount of crack growth nearer the crack center.The higher critical strain energy density value associated with the free surface results in retardation of crack growth near the free surface. A schematic of the resulting crack growth pattern is shown in Figure 27. This is consistent with observed surface crack growth patterns of subjected to tension as reported by McGowan [31] and more recently by Van Stone [22]. It has been noted that surface cracks under tensile fatigue loading will tend to grow towards an aspect ratio of 0.7 to 0.8 [11] with increasing depth; an increase in crack depth with slightly less increase in crack width, as predicted, will lead to this trend.

The strain energy density profile for the semi-circular (a/b=1.0) crack subjected to bending is compared with the critical strain energy density curve in Figure 28. Even though the maximum strain energy density occurs at the free surface fracture initiation will occur at some intermediate angle. Using a bi-linear representation of the critical strain energy density, the point of fracture initiation will be at approximately 60°. The resulting crack growth pattern is shown in Figure 28 and results in the 'butterfly wing' pattern often experimentally observed [32,33], predicted in a LEFM study by a an observed change in the interferometry fringe count indicating a higher potential for crack growth [34] and predicted from experimental results by Ruiz and Epstein [33]. In both [33] and [34] crack growth patterns are established based on experimental results. Prediction of fracture inititation at 60° compares favorably with fracture initiation point predictions of 53° to 66° based on experimental results [34]. Retardation along the free surface is also indicated by the strain energy density contour.

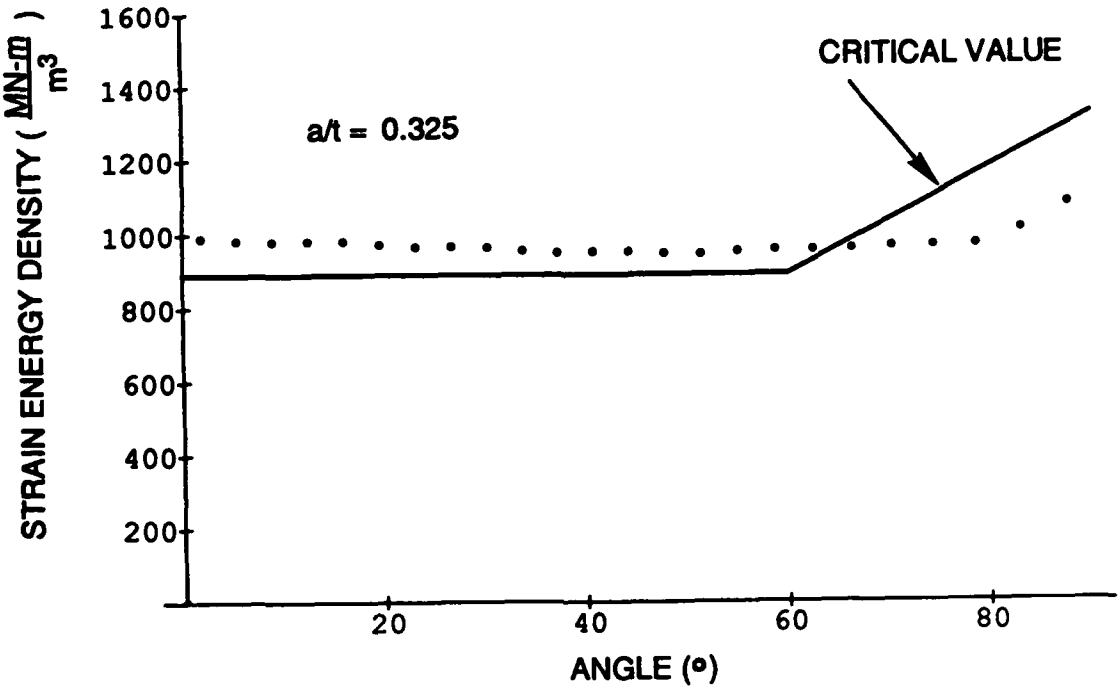

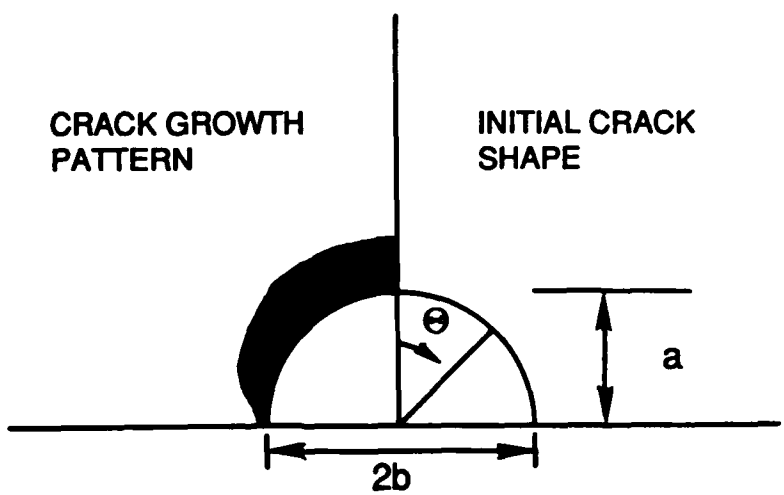

Fig. 27 — Critical Strain Energy Density Profiles and Crack Growth Patterns for Semi-Circular (a/b = 1.0) Cracks In Tension

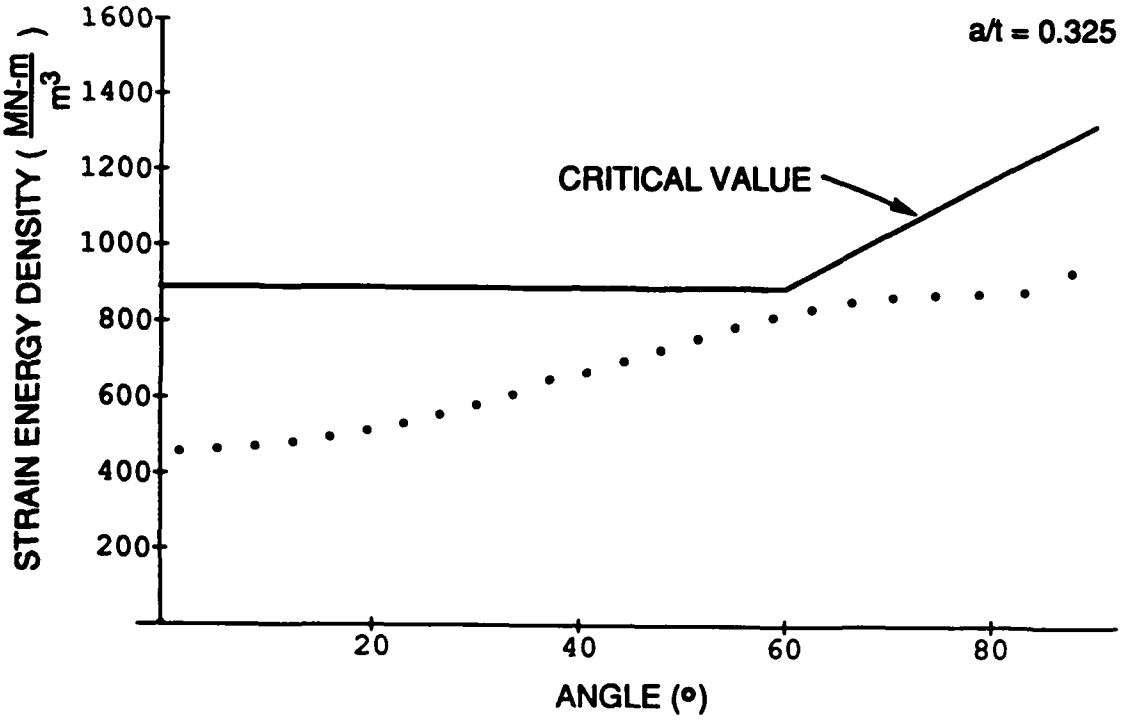

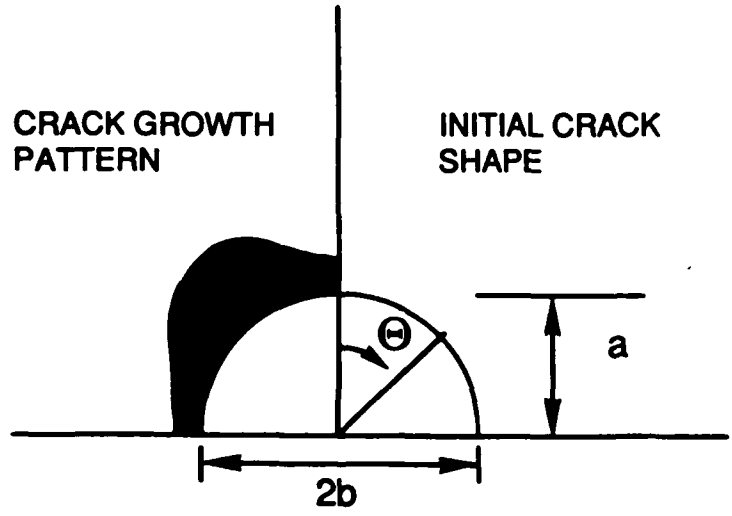

Fig. 28 — Critical Strain Energy Density Profiles and Crack Growth Patterns for Semi-Circular (a/b = 1.0) Cracks In Bending

If an ellipse is drawn which encompasses the 'butterfly wing' crack geometry, the crack growth trend is for a reduced aspect ratio with increasing depth. This is consistent with experimental observations which shown that surface flaws subjected to bending fatigue tend to grow towards an aspect ratio of 0.1 [11].

The strain energy density profile for the semi-elliptical (a/b=0.25) crack subjected to tension is compard with the critical strain energy density profile in Figure 29. The maximum strain energy density occurs at the crack center. This is where the minimum critical strain energy density occurs. The resulting crack growth pattern is shown in Figure 30. Crack growth will occur in the central section of the surface crack. Little or no crack growth will occur near the free surface. This will result in an increase in the aspect ratio with crack growth. This growth pattern will result in higher aspect ratio surface cracks consistent with fatigue crack growth data [11].

The strain energy density profile for the semi-elliptical (a/b=0.25) crack subjected to bending is compared with the critical strain energy density curve in Figure 30. The same pattern as seen for tension loading occurs. The resulting crack growth pattern is shown in Figure 31. Crack growth will occur in the central region of the surface crack. A higher aspect ratio will be the result of crack growth. This is not in conflict with reported fatigue crack growth patterns for surface cracks with aspect ratios between approximately 0.1 and 0.3 and initial crack depth ratios between 0.1 and 0.4 [11]. In these cases, there is an initial increase in aspect ratio before growth along the width directions dominates. The domination of growth along the thickness direction will eventually result in a lower aspect ratio.

It is expected that different initial crack geometries will result in different crack growth patterns. As evidence of this, one can examine the fatigue crack growth patterns presented by Shang-Xian [11] shown in Figure 1. Independent of Shang-Xain, Miyoshi et al [1] noted in their study of leak before break criterion that the initial crack shape was one of the most important features for determining the leak before break criticality of a surface flaw.

Summary

Nonlinear numerical simulations are performed to determine the global and local response of two surface cracks of differing depths due to either tension or bending across the thickness. The surface cracks are embedded

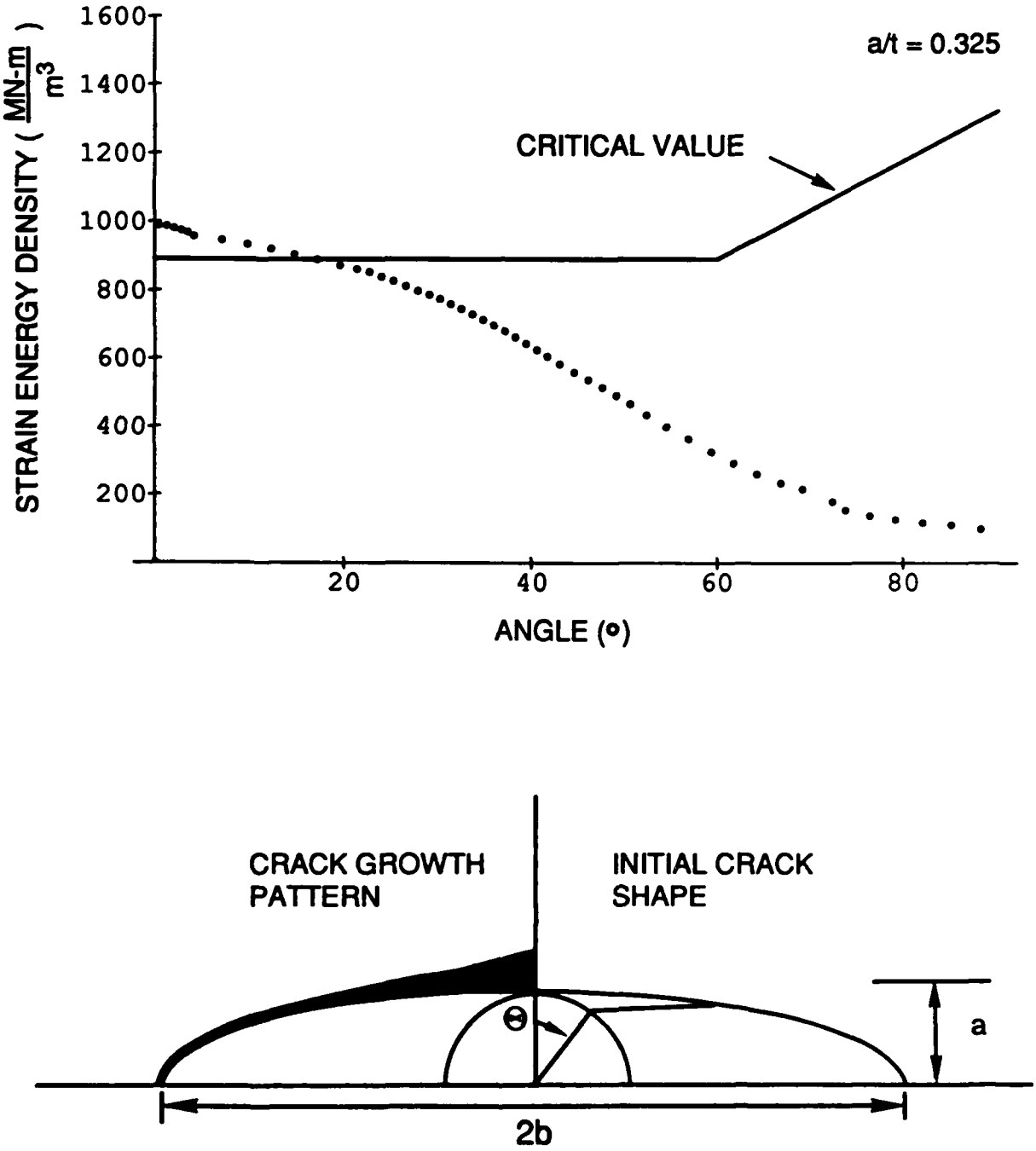

Fig. 29 — Critical Strain Energy Density Profiles and Crack Growth Patterns for Semi-Elliptical (a/b = 0.25) Cracks In Tension

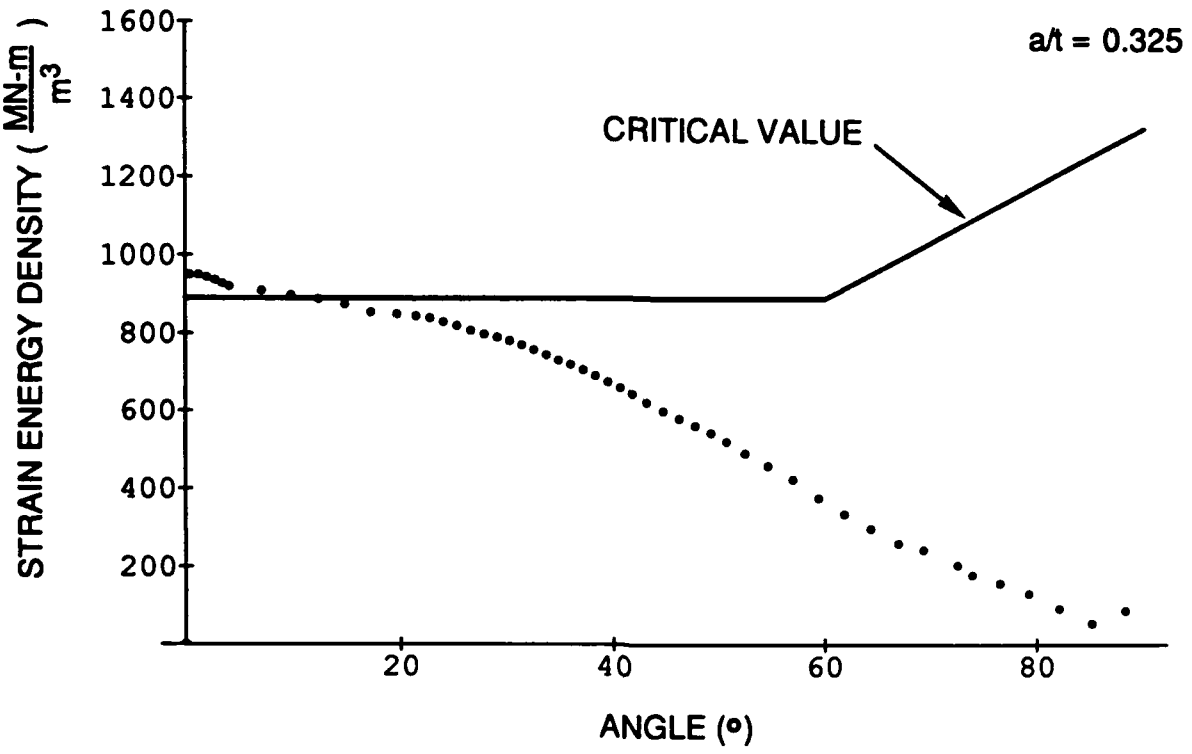

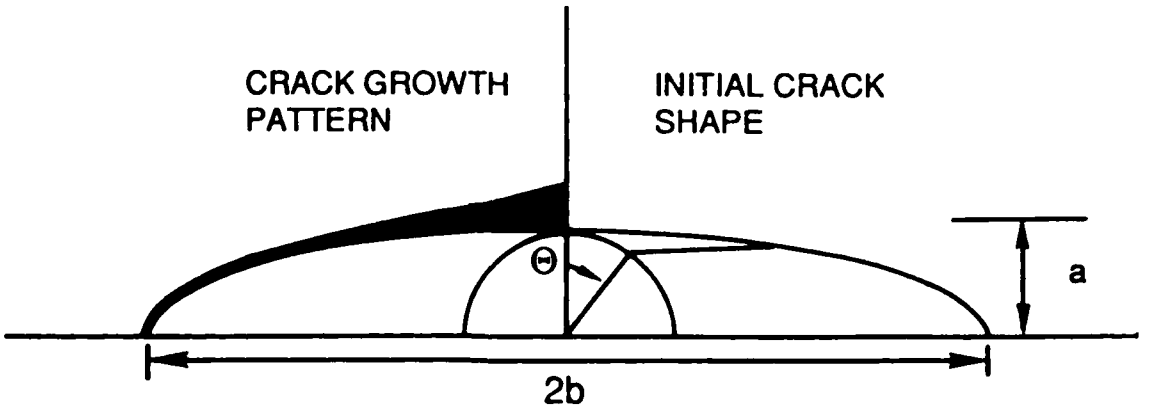

Fig. 30 — Critical Strain Energy Density Profiles and Crack Growth Patterns for Semi-Elliptical (a/b = 0.25) Cracks in Bending

in HY-100 structural steel, a high ductility and toughness metal. The crack geometries and crack depth studied are:

aspect ratios (a/b)- 1.0 (semi-circular) and 0.25 (semi-elliptical)

crack depths (a/t) - 0.25, 0.30 and 0.325

The crack geometries and crack depths chosen are representative of surface cracks of moderate depth. The material response of HY-100 structural steel has been previously characterized for large strain deformation. Failure is defined by a local fracture criterion using critical strain energy density. Differences in constraint along the crack perimeter are taken into account by recognizing the stress-strain history dependence of the critical strain energy density.

Strain energy density profiles were determined along the crack perimeter for each crack geometry, crack depth and loading conditions combination. The patterns of the strain energy density profiles were consistent for each crack geometry and loading conditions. In most cases, similar trends are observed when the strain energy density profiles were compared with typical LEFM fracture criteria profiles.

The strain energy density profiles and the critical strain energy curve based on local constraint history are used to establish fracture inititaion and crack growth patterns. The location of fracture initiation points is not determined a priori. The location of fracture initiation is determined from the combination of the critical strain energy density curve and the calculated strain energy density profile.The resulting fracture initiation points and crack growth patterns are compared with experimental results and observations. The crack growth patterns derived from the numerical simulation accurately predict experimental observations.

In conclusion, it has been demonstrated that the stress-strain dependency of the fracture criterion is equally as important as the variation of the fracture parameter along the curved crack perimeter. Correct crack growth patterns can only be predicted if the effects of variations in constraint are explicitly incorporated into the fracture evaluation.

References

1. Miyoshi, T., Shiratori, M. and Yoshida, Y., "Leak Before Break Evaluation of a Plate with a Surface Crack Subjected to Tension," Engineering Fracture Mechanics, Vol. 24, 1986, pp. 103-110.

2. Little, C. D. and Bunting, P. M., "The Surface Flaw in Aircraft Structures and Related Fracture Mechanics Analysis Problems," The Surface Crack: Physical Problems and Computational Solutions, ASME, 1972, pp.11-42.

3. Collipriest, J. E., Jr.,"An Experimentalist's View of the Surface Flaw Problem, "The Surface Crack: Physical Problems and Computational Solutions, ASME, 1972, pp.43-62.

4. Newman, J. C., Jr. and Raju, R. S.,"Stress-Intensity Factors for Internal and External Surface Cracks in Cylindrical Vessels," Journal of Pressure Vessel Technology, Vol. 104, 1982, pp. 293-298.

5. Kumar, V. and German, M. D., "Nonlinear Analysis of Surface Cracks in Cylinders," Analytical, Numerical and Experimental Aspects of Three Dimensional Fracture Processes, AMD-Vol. 91, ASME, 1988, pp. 63-88.

6. Schmitt, W., Bartholome, G., Grostad, A., and Miksch, M., "Calculation of Stress Intensity Factors of Cracks in Nozzles," International Journal of Fracture, Vol. 12, No. 3, June 1976, pp. 381-390.

7. Smith, T. A. and Warwick, R. G., "A Survey of Defects in Pressure Vessels in the UK for the Period 1962-78 and Its Relevance to Nuclear Primary Circuits," International Journal Pressure Vessel and Piping, Vol. 11, 1983, pp. 127-166.

8. Ochi, Y., Ishii, A. and Sasaki, S. K., "An Experimental and Statistical Investigation of Surface Fatigue Crack Initiation and Growth," Fatigue Fracture Engng. Mater. Struct., Vol. 8, No. 4, 1985, pp. 327-339.

9. Reuter, W. G., et al, "Critical Parameters for Ductile Fracture of Surface Flaws," Engineering Fracture Mechanics, Vol. 19, pp. 159-179, 1980.

10. Jolles, M. and Tortoriello, V., "Geometry Variations During Fatigue Growth of Surface Flaws," Fracture Mechanics: Fourteenth Symposium - Volume 1 - Theory and Analysis, ASTM STP 791, ASTM, 1983, pp. I-297-I-307.

11. Shang-Xian, W., "Shape Change of Surface Crack During Fatigue Growth," Engineering Fracture Mechanics, Vol. 22, 1985, pp. 897-913.

12. Parks, D. M. and Wang, Y. Y., "Elastic-Plastic Analysis of Part-Through Surface Cracks," Analytical, Numerical and Experimental Aspects of Three Dimensional Fracture Processes, AMD-Vol. 91, ASME, 1988, pp. 19-32.

13. Dodds, R. H., Jr. and Read, D. T., "Experimental and Numerical Studies of the J-Integral for a Surface Flaw," Analytical, Numerical and Experimental Aspects of Three Dimensional Fracture Processes, AMD-Vol. 91, ASME, 1988, pp. 1-18.

14. Newman, J. C., Jr. and Raju, R. S., "Stress-Intensity Factor Equations for Cracks in Three Dimensional Finite Bodies Subjected to Tension and Bending Loads," NASA Technical Memo. 85793, April, 1984.

15. Fett, T.,"An Estimation of Local Stress Intensity Factors for Semi-Elliptical Surface Cracks," Engineering Fracture Mechanics, Vol. 34, 1989, pp. 883-890.

16. Saff, C. R. and Sanger, K. B., "Part-Through Flaw Stress Intensity Factors Developed by a Slice Synthesis Technique," Fracture Mechanics: Fifteenth Symposium, ASTM STP 833, ASTM, 1984, pp. 24-43.

17. Gangming, L. and Yongyuan, Z., "Application of Boundary Element Method with Singular and Isoparametric Elements in Three Dimensional Crack Problems," Engineering Fracture Mechanics, Vol. 29, No. 1, 1988, pp. 97-106.

18. Wu, X. R., "Stress Intensity Factors for Half-Elliptical Surface Cracks Subjected to Complex Crack Face Loadings," Engineering Fracture Mechanics, Vol. 19, No. 3, 1984, pp. 387-405.

19. Sommer, E., Hodulak, L. and Kordisch, H., "Growth Characteristics of Part-Through Cracks in Thick Walled Plates and Tubes," Journal of Pressure Vessel Technology, Vol. 99, 1977, pp. 106-111.

20. Hodulak, L, Kordisch, H., Kunzelmann, S. and Sommer, E., "Growth of Part-Through Cracks," Fracture Mechanics, ASTM STP 677, ASTM, 1979, pp. 399-410.

21. Trantina, G., DeLorenzi, H. G. and Wilkening, W. W., "Three Dimensional Elastic-Plastic Finite Element analysis of Small Surface Cracks," Engineering Fracture Mechanics, Vol. 18, 1983, pp. 925-938.

22. Van Stone, R. H., Gilbert, M. S., Gooden, O. C. and Laflen, J. H., "Constraint-Loss Model for the Growth of Surface Fatigue Cracks," Fracture Mechanics: Nineteenth Symposium, ASTM STP 969, ASTM, 1988, 637-656.

23. Dodds, R. H., Jr., Carpenter, W. C. and Sorem, W. A., "Numerical Evaluation of a 3-D J-Integral and Comparison with Experimental Results for a 3-Point Bend Specimen, Engineering Fracture Mechanics, Vol. 29, 1988, pp. 275-285.

24. Nikishkov, G. P. and Atluri, S. N., "Three-dimensional Elastic-Plastic J-Integral Calculations for Semielliptical Surface Cracks in a Tensile Plate, Engineering Fracture Mechanics, Vol. 29, No. 1, pp. 81-87, 1988.

25. Hibbitt, H. D, Karlsson, B. I. and Sorensen, E. P., "ABAQUS User's Manual," Hibbitt, Karlsson and Sorensen, Inc., 1984.

26. Hibbitt, H. D, Karlsson, B. I. and Sorensen, E. P., "ABAQUS Theory Manual," Hibbitt, Karlsson and Sorensen, Inc., 1984.

27. Matic, P., Kirby, G. C. III and Jolles, M. I., "The relation of tensile specimen size and geometry effects to unique constitutive parameters for ductile materials," Proceedings of the Royal Society of London, Vol. A417, 1988, pp. 309-333.

28. DeGiorgi, V. G., Kirby, G. C. III and Jolles, M. I., "Prediction of Classical Fracture Initiation Toughness," Engineering Fracture Mechanics, Vol. 33, 1989, pp. 773-785.

29. PDA Engineering, PATRAN User's Manual, PDA Engineering, Santa Ana, CA, 1987.

30. Francis and Davidson, "Experimental Study of Plastic Yielding at the Tip of Surface Flaw Cracks," NASA-CR-114934, Southwest Research Institute, 1971.

31. McGowan, J. J., "An Overview of Current Methods Used For Assessing Surface Flaws in Nuclear Reactor Vessels," Nuclear Engineering and Design, Vol. 73, 1982, pp. 275-281.

32. Smith, C. W., "Stress Intensity and Flaw Shape Variations in Surface Flaws," Experimental Mechanics, April, 1980, pp. 126-133.

33. Ruiz, C. and Epstein, J., "On the Variation of the Stress Intensity Factor Along the Front of a Surface Flaw," International Journal of Fracture, Vol 28, 1985, pp. 231-238.

34. Gensheimer, V. M. and Packman, P. F.,"Variation in Stress-Intensity Factor and Back-Surface Displacement for Surface Cracks", Experimental Mechanics, June, 1988, pp. 182-187.